https://doi.org/10.5194/bg-2022-216
Preprint. Discussion started: 21 November 2022

Biogeosciences
Discussions
Open Access

Seasonal and interannual variability of the pelagic ecosystem and of the organic carbon budget in the Rhodes Gyre (Eastern Mediterranean): influence of winter mixing

Joelle Habib[1,2], Caroline Ulses[1], Claude Estournel[1], Milad Fakhri[2], Patrick Marsaleix[1], Mireille Pujo-Pay[3], Pascal Conan[3], Marine Fourrier[4], Laurent Coppola[4,5], Alexandre Mignot[6], Laurent Mortier[7]

[1] Laboratoire d'Etudes en Géophysique et Océanographie Spatiales (LEGOS), Université de Toulouse, CNES/CNRS/IRD/UT3, Toulouse, France

[2]National Center for Marine Sciences, National Council for Scientific Research (CNRS-L), Jounieh, Lebanon

[3]Sorbonne Université, CNRS, UMR7621, Laboratoire d'Océanographie Microbienne (LOMIC), Paris, France

[4] Laboratoire d'Océanographie de Villefranche, CNRS, Sorbonne Université, Villefranche-sur-Mer, France

[5]Sorbonne Université, CNRS, OSU STAMAR, UAR2017, 4 Place Jussieu, 75252 Paris cedex 05, France

[6]Mercator Océan International, Toulouse, France

[7]Sorbonne Université, UPMC Univ Paris 06 CNRS-IRD-MNHN, Laboratoire d'Océanographie et du Climat: Expérimentations et Approches Numériques (LOCEAN), 4 place Jussieu, 75005 Paris, France

Correspondence to: Joëlle Habib (joellehabib22@hotmail.com)

Abstract

The Rhodes Gyre is a cyclonic persistent feature of the general circulation of the Levantine Basin in the eastern Mediterranean Sea. Although it is located in the most oligotrophic basin of the Mediterranean Sea, it is a relatively high primary production area due to strong winter nutrient supply associated with the formation of Levantine Intermediate Water. In this study, a 3D coupled hydrodynamic-biogeochemical model (SYMPHONIE/Eco3M-S) was used to characterize the seasonal and interannual variability of the Rhodes Gyre's ecosystem and to estimate an annual organic carbon budget over the 2013-2020 period. Comparisons of model outputs with satellite data and compiled in situ data from cruises and BioGeoChemical-Argo floats revealed the ability of the model to reconstruct the main seasonal and spatial biogeochemical dynamics of the Levantine Basin. The model results indicated that during the winter mixing period, phytoplankton first progressively grow sustained by nutrient supply. Then, short episodes of convection driven by heat loss and wind events, favoring nutrient injections, organic carbon export and inducing light limitation on primary production, alternate with short episodes of phytoplankton growth. The estimate of the annual organic carbon budget indicated that the Rhodes Gyre is an autotrophic area with a positive net community production in the upper layer (0-150 m) amounting to 31.2 ± 6.9 g C m^{-2} $year^{-1}$. Net community production in the upper layer is almost balanced over the seven year period by physical transfers, (1) via downward export (16.8 ± 6.2 g C m^{-2} $year^{-1}$) and (2) through lateral transport towards the surrounding regions (14.1 ± 2.1 g C m^{-2} $year^{-1}$). The intermediate layer (150-400 m) also appears to be a source of organic carbon for the surrounding Levantine Sea (7.5 ± 2.8 g C m^{-2} $year^{-1}$) mostly through the subduction of Levantine Intermediate Water following winter mixing. The Rhodes Gyre shows high interannual variability with enhanced primary production, net community production and exports during years marked by intense heat losses and deep mixed layers. However, annual

https://doi.org/10.5194/bg-2022-216
Preprint. Discussion started: 21 November 2022

primary production appears to be only partially driven by winter vertical mixing. Based on our results, we can speculate that future increase of temperature and stratification could strongly impact the carbon fluxes in this region.

1 Introduction

The ocean absorbs about 25% of the anthropogenic CO_2 emitted into the atmosphere (Friedlingstein et al., 2021). Various processes are involved in the ocean carbon sink: chemical processes driving the air-sea exchanges according to CO_2 solubility linked to sea surface temperature and salinity, biogeochemical processes in which dissolved inorganic carbon is first converted into organic carbon through photosynthesis, and then transferred to great depths, possibly after further transformations, and diffusive and advective physical processes (Palevsky and Quay, 2017; Palevsky and Nicholson, 2018). Those various chemical, biogeochemical and physical mechanisms interact, especially in highly dynamical regions such as water formation areas (Körtzinger et al., 2008), and it is crucial to understand those mechanisms and their interactions, as well as their variability and evolution in the context of increasing atmospheric CO_2 content and global warming.

The Levantine Basin, in the southeastern Mediterranean Sea (Fig. 1), is a concentration basin, i.e. there is a net loss of water by evaporation, balanced by an input of less salty water from the Atlantic Ocean flowing successively through the straits of Gibraltar and Sicily (Lascaratos et al., 1993). The Levantine Basin is also a warm and salty sea with surface temperature reaching 25 °C and salinity above 39.5 (Manca et al., 2004). Located in the northeastern part of the Levantine Basin, the Rhodes Gyre (Fig. 1) is a cyclonic persistent feature (Robinson et al. 2001; Millot and Taupier-Letage, 2005; Estournel et al., 2021) whose hydrodynamics has been well described in the literature, in particular following the POEM program in the 90s (Theocharis et al., 1993; Ozsoy et al., 1991; 1993; Marullo et al., 2003). During cold winter wind events, the high saline surface waters of the cyclonic Rhodes Gyre cool down, and their density increases, which generates deep mixing layers. During the following months, the newly formed dense water sinks to reach intermediate depths (130 - 400 m) forming the Levantine Intermediate Water (LIW, Hecht et al., 1988; Taillandier et al., 2022). Other studies have also reported LIW formations in the Gulf of Antalya (Sur et al., 1992; Kubin et al., 2019; Fach et al., 2021), in the southeastern margins of the basin or along the continental margins of the totality of the Levantine Basin (Brenner et al., 1991; Lascaratos et al. 1993; Özsoy et al. 1993). However, the Rhodes Gyre remains the major area of LIW formation in the Levantine Basin (Lascaratos et al. 1999; Özsoy et al., 1989).

From a biogeochemical point of view, the eastern Mediterranean is a singular basin in terms of its oligotrophic to ultra oligotrophic regimes (Krom et al., 1991; Siokou-Frangou et al., 2010; Pujo-Pay et al., 2011; Kress et al. 2014) with chlorophyll concentrations reaching at most 0.5 mg m^{-3} in the deep chlorophyll maximum layer (Mignot et al., 2014). Considered an “oasis” in the Levantine Basin (Siokou-Frangou et al., 1999), the Rhodes Gyre is characterized by higher phytoplankton biomass and biological production than the surrounding region (Vidussi et al., 2011). Yilmaz and Tugrul (1998) detailed the coupling of hydrodynamic conditions and nutrient enrichment in the gyre. Under prolonged and cold winter conditions, the Rhodes Gyre presents chimney formations, where Levantine deep or intermediate water, moving to the surface due to mixing, enriches the euphotic layer in nutrients (Yilmaz and Tugrul, 1998; Ediger and Yilmaz, 1996). Observational studies also showed that cyclonic features of the Rhodes Gyre determine the depth and thickness of the nutricline (Yilmaz et al., 1994). Ediger and Yilmaz (1996) highlighted interannual variability in nutrient supply into the euphotic

https://doi.org/10.5194/bg-2022-216
Preprint. Discussion started: 21 November 2022

layer in the area, with fewer injections during mild winters compared to cold winters. This was in agreement with the one-dimensional coupled physical-biological modeling study by Napolitano et al. (2000) who found an increase of nutrient supply with the intensification of winter cooling across the same year. They also showed that the vertical extent of mixing influences the magnitude and timing of the spring phytoplankton bloom. Based on an analysis of ocean color satellite data, D'Ortenzio and Ribera d'Alcalà (2009) classified the Rhodes Gyre as a trophic regime with an intermittent phytoplankton bloom. They reported a strong interannual variability in the spatial shape and timing of the bloom. Mayot et al. (2016) further showed the alternation between bloom, intermittent and no bloom regimes in the gyre.

After its formation, LIW spreads throughout the whole eastern Mediterranean Sea (Theocharis et al., 1993; Millot and Taupier-Letage, 2005; Estournel et al., 2021) and then heads towards the western Mediterranean and represents the main contribution to the outflow at the Strait of Gibraltar (Tanhua et al., 2013; Malanotte-Rizzoli et al., 2014). LIW is considered to play an important role in the formation of the Mediterranean intermediate and deep waters in the Aegean Sea, as well as in the southern Adriatic Sea and the northwestern Mediterranean Sea (Grignon et al., 2010; Velaoras et al., 2014; Margirier et al., 2020; Taillandier et al., 2022). This water mass may also have a critical impact on the biogeochemistry of the entire Mediterranean Sea (Astraldi et al., 1999; Malanotte-Rizzoli et al., 2014; Kress et al., 2014; Touratier and Goyet, 2009; Palmiéri et al., 2015). Thus, understanding of its formation and propagation is a key to study its impact on biogeochemical dynamics first in the ultra oligotrophic Levantine Basin and then in the entire Mediterranean Sea.

In spite of the importance of LIW in the hydrodynamics and biogeochemistry of the eastern and western Mediterranean Sea, relatively few studies have been conducted since the POEM program in the 90s (The POEM group, 1992), partly because of the complex geopolitical situation and restricted access. In particular, in situ cruise data remain rare in the Rhodes Gyre (Napolitano et al., 2000; Marullo et al., 2003), with most studies having been conducted in the northeastern Levantine Basin (Krom et al., 2005; Hassoun et al., 2019; Alkalay et al., 2020; Fach et al., 2021) or through a limited section in the basin (Moutin and Raimbault, 2002; Pujo-Pay et al., 2011; Santinelli, 2015), and mostly during the stratification period. On the other hand, only one 1-D coupled hydrodynamic-biogeochemical model has been carried out in the Rhodes Gyre (Napolitano et al., 2000), while most 3D modeling studies investigated the whole Mediterranean Sea (Lazzari et al., 2012; Macias et al., 2014; Guyennon et al., 2016; Richon et al., 2017, 2018; Karaloni et al., 2020; Cossarini et al., 2021) or eastern Mediterranean Sea (Petihakis et al., 2009) without focusing on the LIW formation region of the Rhodes Gyre.

Along with the deployment of Argo floats in the Levantine Sea since 2015 (Pasqueron de Fommervault et al., 2015), the PERLE (Pelagic Ecosystem Response to deep water formation in the Levant Experiment) project, within the framework of which this study takes place, was conducted in order to obtain a better understanding of the formation and spreading of LIW and their impacts on the distribution of nutrients and planktonic ecosystems. In the frame of the PERLE project D'ortenzio et al. (2021) documented, using Biogeochemical-Argo floats and in situ data sampled during the cruise, a coupling between mixed layer and phytoplankton dynamics in the Rhodes Gyre. They found that deepening of the mixed layer induces a steady injection of nitrate into the surface followed by a rapid accumulation of phytoplanktonic biomass.

The present study aims to gain insight into carbon dynamics through the examination of seasonal and interannual variabilities of the biogeochemical and physical fluxes of organic carbon, under particulate and dissolved forms, in the Rhodes Gyre and the estimate of an annual budget of organic carbon in the area over a

https://doi.org/10.5194/bg-2022-216
Preprint. Discussion started: 21 November 2022

multi-annual period. For that, we use a 3D hydrodynamic-biogeochemical coupled modeling, over the period from December 2013 to April 2021.

2 Material and methods

2.1 The coupled physical-biogeochemical model

The biogeochemical model Eco3M-S forced offline by daily outputs of the 3D hydrodynamic model SYMPHONIE was the main tool used in the current study.

2.1.1 The hydrodynamic model

The 3D primitive equation ocean model SYMPHONIE is described in detail in Marsaleix et al. (2006; 2008), Estournel et al. (2016) and Damien et al. (2017). This model has been primarily used to describe the circulation in response to wind forcing and the dynamics of river plumes (Estournel et al., 1997, 2001; Marsaleix et al., 1998), coastal circulations (Estournel et al., 2003; Petrenko et al., 2008), dense water formation (Estournel et al., 2005; Ulses et al., 2008; Herrmann et al., 2008; Estournel et al., 2016) and shelf-slope exchanges (Mikolajczak et al., 2020).

2.1.2 The biogeochemical model

Eco3M-S is a biogeochemical multi-nutrient and multi-plankton functional type model, representing the dynamics of the pelagic planktonic ecosystem previously described by Auger et al. (2011) and Ulses et al. (2021). It describes the cycles of carbon (C), nitrogen (N), phosphorus (P), silicon (Si), dissolved oxygen (O_2) and chlorophyll (Chl). The model is composed of eight compartments: dissolved inorganic nutrients (nitrate, ammonium, phosphate and silicate), dissolved oxygen, phytoplankton represented by three size classes (pico-, nano- and micro-phytoplankton), zooplankton formed of three size classes (nano-, micro- and meso-zooplankton), bacteria, particulate organic matter (POM), divided into two groups based on their settling speed (fast and slow settling speed) and dissolved organic matter (DOM). A summary diagram of the food web structure of the model and the interactions between the compartments is represented in Fig. S1.

The model was previously used in the Mediterranean Sea to study the pelagic ecosystem and biogeochemical processes in coastal areas (Auger et al. 2011; Many et al. 2021) and open-sea regions (Herrmann et al. 2013; Auger et al. 2014; Kessouri, 2015; Ulses et al. 2016; Kessouri et al. 2017; 2018; Ulses et al., 2021).

2.1.3 Implementation

The model configuration and implementation of the hydrodynamic simulation were described by Estournel et al. (2021). The model domain covers the Mediterranean Sea as well as the Marmara Sea and reaches 8° West in the Gulf of Cadiz. The horizontal grid is characterized by a resolution that varies between 2.3 and 4.5 km from the northwest to the southeast to account for the increase of the Rossby deformation radius therefore allowing an adequate representation of mesoscale processes. As for the Gibraltar Strait, a narrowing was conducted with a 1.3 km grid for a better representation of the exchange area between the Mediterranean Sea and Atlantic Ocean. The vertical grid uses a VQS (vanishing quasi sigma) coordinate system with 60 levels and closer levels ranging near the surface. This model configuration was used to describe the surface and intermediate water circulations in the eastern Mediterranean Sea (Estournel et al., 2021).

https://doi.org/10.5194/bg-2022-216
Preprint. Discussion started: 21 November 2022

The SYMPHONIE simulation runs from 1 July 2011 to 2 May 2021. The meteorological parameters (with radiative fluxes) are hourly operational forecasts based on ECMWF 12 hour analyses at 1/8° horizontal resolution. A total of 142 rivers (Fig. S2) are considered in the model. As for the rivers of the Levantine Basin, monthly discharges were based on the study of Poulos et al. (1997), except for the Nile River where the discharge value was set to 475 $m^3 s^{-1}$, following Nixon (2003).

We used the daily 3D current velocity, temperature, salinity and vertical diffusivity outputs of the hydrodynamic simulations as forcing fields for the biogeochemical model run. The biogeochemical model runs for the period from 15 August 2011 to 2 May 2021. We initialized the biogeochemical model with observation profiles averaged over 10 regions of the Mediterranean Sea (indicated in Fig. S2). For inorganic nutrients profiles, we used the CARIMED (CARbon, tracer and ancillary data In the MEDsea database (Àlvarez et al., 2019; see Sect. 2.2.2), considering only summer data over the period 2011-2012 since the simulation starts in August. Regarding the dissolved oxygen and chlorophyll concentrations, we initialized using summer in situ observations from BioGeoChemical-Argo floats (BGC-Argo, Argo, 2022) (see Sect. 2.2.3) and the CARIMED database. Solar radiation and wind forcing for the biogeochemical simulation are those used for the hydrodynamic simulation. Atmospheric depositions of inorganic nutrients were taken into account. Nitrate atmospheric depositions were applied as constant values based on the results of Kanakidou et al. (2012), Ribera d'Alcala et al. (2003), Powley et al. (2017) and Richon et al. (2018) and silicate deposition was prescribed as constant values for western (west of the Sicily Strait) and eastern basins based on estimates given by Ribera d'Alcalà et al. (2003). We deduced phosphate deposition from monthly Saharan dust deposition modeled with the regional model ALADIN-Climat (Nabat et al., 2015) and averaged over the period 1979-2016. We hypothesized that phosphorus represents 0.07 % of dust and that 15% is in soluble form (Herut and Krom, 1996; Guerzoni et al., 1999; Ridame and Guieu, 2002; Richon et al., 2017). Nutrient fluxes at the water column/sediment interface have been obtained through a coupling of the biogeochemical model with a simplified version of the vertically integrated benthic model described by Soetaert et al. (2000). At the river mouths, concentrations of nutrients were imposed at subbasin scale using the dataset of Ludwig et al. (2010). In the Atlantic Ocean, nutrients were prescribed using monthly profiles from the World Ocean Atlas 2009 climatology (https://odv.awi.de/en/data/ocean/world-ocean-atlas-2009/) at 5.5 °W. In the Marmara Sea, in order to represent a two-layer flow regime, we imposed a relaxation with a timescale of 1 day towards nitrate concentrations of 0.24 and 1.03 mmol N m^{-3} and phosphate concentrations of 0.06 and 0.05 mmol P m^{-3} for depths above and below 15 m respectively, based on the observations near the Dardanelles Strait from Tugrul et al. (2002).

2.1.4 Definition of the study area and budget calculation

Previous studies determined the Rhodes Gyre's location based on a Sea Surface Temperature (SST) criteria. Marullo et al. (2003) using AVHRR (Advanced Very High-Resolution Radiometer) images time series located the gyre in an area between the southeast of Rhodes and the east of Crete: 27°-30° E and 34-36° N with a threshold of 14°C. D'Ortenzio et al. (2021) identified the region using a SST threshold at 15°C based on satellite images. Other studies have also used the Sea Surface Height (SSH) from ADT (Absolute Dynamical Topography) maps to detect mesoscale features of the Mediterranean Sea such as Cornec et al. (2021).

https://doi.org/10.5194/bg-2022-216
Preprint. Discussion started: 21 November 2022

In this study, we defined the Rhodes Gyre area based on modeled SSH as well as on modeled surface density. The winter mean for both parameters was calculated between January and mid-March during the period generally associated with deep vertical mixing (Malanotte-Rizzoli et al., 2003). We set a minimum threshold at 28.8 kg m^{-3} for density anomaly and a maximum of -0.3 m for SSH, based on Kubin et al. (2019). The position of the region respecting the set of criteria varying from year to year, we chose the smallest outline in order to cover the most of the gyre during the period of study. The resulting region (indicated in Fig. S3 and Fig. 1) designates a large area of the Rhodes Gyre, covering 27 500 km^2, that includes areas where the strongest mixing occurred over the period 2014-2021. The hydrodynamic and the biogeochemical variables presented in the following sections correspond to values averaged over this domain.

To calculate the organic carbon budget, the water column was divided into two layers. The surface layer is defined as the euphotic layer covering the surface to 150 m of depth, and the intermediate layer, from 150 to 400 m (Ozer et al., 2016; Menna et al., 2010, 2021), includes the LIW. Organic carbon englobes dissolved and particulate organic carbon (DOC and POC, respectively). The latter includes all modeled components of POC: low and fast sinking detritic particles and living organisms, i.e. the three size classes of phytoplankton, the three size classes of zooplankton and bacteria. The biogeochemical contribution to the organic carbon budget is the sum of gross primary production (GPP) and organic carbon consumption through community respiration (CR) (phytoplankton, zooplankton and bacteria respiration) (see Table S4 in Supplement Material by Many et al. (2021)). The physical contribution of the budget is divided into two components: lateral transport and vertical transport, both due to mixing and advection. Lateral transport represents the net transport at the lateral limits of the Rhodes Gyre area. Vertical transport represents the exchanges at the vertical boundaries of the layer. Positive values correspond to fluxes of organic carbon that enters the considered layer of the Rhodes Gyre area. Similarly, negative values correspond to fluxes of organic carbon that leaves the considered layer of the Rhodes Gyre area. The internal variation of organic carbon inventory, biological term and lateral physical term were calculated online, while the vertical term was calculated as the residual based on values of all other terms. The equations of the budget are given in Supplement Material (Text S1).

2.2 Observations used for the coupled model assessment

In order to assess the performance of the model, we used remote sensing, in situ and BGC-Argo float data over the study period. Because the Rhodes Gyre area was limited in terms of observations, the comparison was conducted all over the Levantine Basin. The spatial coverage of the in situ dataset used in this study is shown in Fig. 1.

2.2.1 Satellite Data

To evaluate the modeled surface chlorophyll concentration, we used daily level 4 reprocessed data obtained from the European Copernicus Marine Environment monitoring Service (CMEMS) from the website (http://resources.marine.copernicus.eu/, products: OCEANCOLOUR_MED_CHL_L4_REP_OBSERVATIONS_009_078, last access: 16 June 2022) with a spatial resolution of 1 km. The latter is a regional product with daily interpolated chlorophyll concentrations from multi sensors (MODIS-Aqua, NOAA-20-VIIRS, NPP-VIIRS, MERIS sensors). To compare model results with those data, we interpolated the data on the model grid.

2.2.2 Cruise observations

We used the CARIMED (CARbon, tracer and ancillary data In the MEDsea) database with 862 profiles covering cruise observations available in the Mediterranean Sea for the period 2011-2018 (Àlvarez et al., 2019), to complete the assessment of the spatial distribution of the simulated variables. Data passed two quality controls following the GLODAP (Global Data Analysis Project) procedure (Key et al., 2004) adapted to the Mediterranean Sea. This dataset included cruises with only best-practiced standards for nutrients following the GO-SHIP (The Global Ocean Ship-based hydrographic investigations Program) and the WOCE (World Ocean Circulation Experiment) protocols. Fourrier et al. (2020) added data from 10 other cruises to the dataset and validated them. The data are available on figshare (https://doi.org/10.6084/m9.figshare.12452795.v2, last access: 10 October 2022, Fourrier, 2020). Sea water was collected using Niskin bottles from the surface to 4600 m of depth. An SBE43 oxygen sensor was used during the cruises and adjusted with Winkler measurements. The inorganic nutrients were determined following the colorimetric methods of Grasshoff et al. (1999).

We also used the PERLE cruise dataset: PERLE 1 (25 profiles) covering the Levantine Basin in October 2018 and PERLE 2 (29 profiles) in February-March 2019 (D'Ortenzio et al., 2021). At all stations water samples were collected from Niskin bottles for nutrient analysis. This dataset passed a primary quality control.

It is important to mention that we used validation data different from calibration data to prevent over fitting of model parameters and to have a better assessment of the model's reaction capacity when the validation patterns are different from those used in the calibration; this method was supported by Robson (2014) .

2.2.3 BGC-Argo floats

To evaluate the temporal and the spatial variability of the modeled dissolved oxygen and chlorophyll, we used observations from BGC-Argo floats providing O_2 (1566 profiles) and Chl-a (1171 profiles) measurements (Argo, 2022) deployed in the eastern Mediterranean, downloaded from the Argo Global Data Assembly Center web portal accessible through the Coriolis database (http://www.coriolis.eu.org, last access: 21 June 2022). Regarding O_2 measurements made by Argo floats, air measurements and optode calibration protocols have led to a significant improvement in the quality and accuracy of these data (Bittig et al. 2018; Bittig and Körtzinger 2015). These can now reach accuracies of 1-1.5 µmol kg^{-1} close to those achieved in situ by the Winkler method. Mignot et al. (2019) conducted a similar study to try to quantify the observational errors for dissolved oxygen and chlorophyll concentrations. They found a bias of 2.9 ± 5.5 µmol kg^{-1} and -0.06 ± 0.02 mg m^{-3} for the oxygen and the chlorophyll respectively and a relative Root Mean Square Difference (RMSD) of 6.1% for oxygen and 5.4 % for chlorophyll in the Mediterranean Sea.

3 Results

3.1 Assessment of the coupled physical-biogeochemical model

The hydrodynamical model was evaluated and validated by Estournel et al. (2021) by computing model/observations statistics using salinity and temperature observations from Argo floats and satellite data. The authors showed the ability of the model to reproduce the hydrological characteristics of the surface and intermediate waters in the eastern Mediterranean Sea. In the following section, we focus on the evaluation of the biogeochemical model in the Levantine Sea.

https://doi.org/10.5194/bg-2022-216
Preprint. Discussion started: 21 November 2022

3.1.1 Surface chlorophyll concentration

Figure 2 shows the temporal variation of the satellite and modeled surface chlorophyll averaged all over the Levantine Sea (panel (a)), as well as the BGC-Argo float data, and the modeled surface chlorophyll along the trajectory of floats located in the Levantine Sea (panel (b), data located specifically in the Rhodes Gyre are indicated in lighter colors), over the study period. To quantify the differences between model outputs and observations, we calculated the percent bias (PB, $100 \times \frac{Mean\,mod - Mean\,obs}{Mean\,obs}$, where *Mean mod* and *Mean obs* are the mean of the model outputs and observations respectively) and the Normalized Root Mean Square Difference (NRMSD, $\frac{\sqrt{\square^{\square}_{\square}}}{\square}$, where *Obs* and *Mod* are the observation and model output, respectively, *Max obs* and *Min obs* are the maximum and minimum observation values for the chlorophyll).

The model captures the seasonal dynamics of the observed satellite chlorophyll (Fig. 2a). At the end of fall, the chlorophyll concentration begins to increase progressively and reaches its maximum in February/March. The surface concentration is minimal in summer, for both the model and satellite. The model and satellite show differences in magnitude: in the model the winter maximum is generally higher, and the summer minimum values are lower, compared to the satellite data. The standard deviation (SD) of the model (0.04 mg Chl m^{-3}) is close to the mean chlorophyll concentration (0.05 mg Chl m^{-3}) which underlines the high variability of this oligotrophic system. The mean surface chlorophyll concentration in the satellite data is 0.05 ± 0.02 mg Chl m^{-3}. We obtain a highly significant correlation coefficient equal to 0.90 (p-value < 0.01), and low values for the NRMSD (23%) and percent bias (-0.71%), between model outputs and satellite data over the whole study period.

Regarding the comparison with BGC-Argo float data in the Levantine Sea and the Rhodes Gyre, the model reproduces correctly both the seasonal cycle and the magnitude of chlorophyll during the different periods of the year. Both model and float data show high variability in late winter/early spring in the Rhodes Gyre in agreement with previous studies (D'Ortenzio and Ribera d'Alcalà, 2009; Salgado-Hernanz et al., 2019; Kotta and Kitsiou, 2019). The statistical metrics show a significant correlation equal to 0.73 (p-value <0.01) between the observed and modeled values in the Levantine Sea. The NRMSD is equal to 13% and the percent bias remains low (-16%). Similar statistical scores were obtained between the model outputs and the float data in the Rhodes Gyre, i.e. correlation (0.78, p-value <0.01) as well as low bias (-23%) and NRMSD (8%). The difference between the comparisons of model results with satellite data and those with BGC-Argo float data could be attributed in part to an underestimation in winter of chlorophyll concentration in satellite data in the Levantine Sea as suggested by Vidussi et al. (2001) and reported by D'Ortenzio et al. (2021).

3.1.2 Seasonal variation of vertical distribution

Figure 3 shows a comparison of modeled and observed mean seasonal profiles of chlorophyll, dissolved oxygen, nitrate and phosphate, in the Levantine Sea from both BGC-Argo floats and the oceanographic cruises. The model results are compared with the observations at the same dates and positions. This comparison is completed by a statistical analysis computed over the whole period of study (Fig. S4).

The model reproduces the general features of the nitrate and phosphate concentration profiles with an increase from the surface to 500-1000 m and a gradual, low decrease below (Fig. 3). The modeled phosphate and nitrate

https://doi.org/10.5194/bg-2022-216
Preprint. Discussion started: 21 November 2022

concentrations in the transitional layer (500-1000), located between the intermediate and deep layers, are in the lower range values of observations.

The statistical analysis (Fig. S4) shows that the model displays high correlation ($R > 0.90$, p-value < 0.01, for all the cruise datasets) and low RMSD (~ 0.01, 0.03 and 0.02 mmol P m^{-3} for CARIMED, PERLE 1 and PERLE 2, respectively) and bias (0.006,-0.01 -0.03 mmol P m^{-3} for CARIMED, PERLE 1 and PERLE 2, respectively) compared to the phosphate observations. PERLE 1 and PERLE 2 phosphate observations show high variability, with a SD ~ 0.065 and 0.062 mmol P m^{-3} respectively. The modeled SD for both cruises is slightly smaller in comparison with observations (0.05 and 0.04 mmol P m^{-3}). As for nitrate, the metrics confirm the good agreement between model outputs and observations with significant correlations above 0.95 (p-value < 0.01), a bias of 0.1, -0.1 and 1.4 mmol N m^{-3} for PERLE 1, PERLE 2 and CARIMED, respectively, and a centered RMSD close to 0.4 mmol N m^{-3} for PERLE 1 and PERLE 2 and 0.5 mmol N m^{-3} for CARIMED.

The model reproduces the development of a deep chlorophyll maximum (DCM) in spring, and its presence in summer and fall, reaching a maximal depth in summer (Fig. 3). During winter, the model overestimates the surface chlorophyll by 0.05 mg Chl m^{-3} and homogenization in the first 50 m. It generally underestimates the DCM concentration by 25 % and overestimates its depth by 20 m (130 m and 110 m for the model and the float, respectively).

The magnitude and seasonal variation of the vertical profile of dissolved oxygen concentration are well reproduced (Fig. 3). In winter, the surface oxygen concentration is maximal coinciding with the peak of surface chlorophyll. It reaches 230 µmol kg^{-1} and 240 µmol kg^{-1} for the model and the float data respectively. The model reproduces the presence of a subsurface oxygen maximum in spring, summer and fall, between 40 and 60 m depth as observed, with an underestimation of its concentration by 10 µmol kg^{-1}. The oxygen minimum layer concentration stands within the range of the observed values. The model is highly correlated with the different data sets ($R > 0.95$, p-value < 0.01). The observations show a SD close to 16.5 µmol kg^{-1} for the floats. The modeled float oxygen concentrations also show a high SD of ~ 14.5 µmol kg^{-1}.

3.1.3 Study case: BGC-Argo float/model comparison

Figure 4 represents the evolution of the chlorophyll and oxygen concentrations for Float 6901764 and those extracted from the model at the same time and location (both indicated on panel (b)). The choice of the float was done based on both the temporal extension and the localization of the platform: this float covers both the Rhodes Gyre and the surrounding region for a long period, 2015 – 2019 (Fig. 4b). The model represents the seasonal cycle, with an increase in the surface chlorophyll during winter (Fig. 4d) followed by the formation and deepening of the DCM (Fig. 4a). The DCM is mostly well localized in the model (10-20 m deeper than in the observations during summer). The model accurately reproduces the vertical distribution of chlorophyll although some differences exist, such as the slight underestimation of the intensity of the maximum chlorophyll also noted in Fig. 3. The surface chlorophyll concentrations for the first 10 m from the simulation and the float data (Fig. 4d) are significantly correlated ($R=0.83$, p-value < 0.01).

The modeled and observed oxygen display a similar seasonal cycle, with an increase in surface oxygen concentration during winter (Fig. 4e) followed by a decrease at the surface and a deepening of the oxygen maximum (Fig. 4c) during the stratification period. In both the model outputs and observations the oxygen

https://doi.org/10.5194/bg-2022-216
Preprint. Discussion started: 21 November 2022

minimum layer is located, at depths between 300 and 1000 m. The model and the float show a good temporal correlation for the surface concentration of dissolved oxygen (R=~0.96, p-value < 0.01, Fig. 4e).

3.2 Meteorological and hydrodynamic variability

Figure 5 exhibits the time series of surface heat fluxes, mixed layer depth (MLD) and temperature profile anomaly (computed based on the difference in temperatures from the mean daily temperature over the seven years), spatially averaged over the Rhodes Gyre area (defined in Sect. 2.1.4). The mixed layer depth is defined as the depth where the potential density exceeds by 0.01 kg m^{-3} its value at 10 m depth (Coppola et al., 2017). This density based criteria is more appropriate than shallower temperature-based MLD estimates to represent mixing in the dense water formation zone, such as the Rhodes Gyre, as suggested by Houpert et al. (2015).

The domain displays a seasonal cycle, characterized by a heat loss at the air-sea interface from October to March followed by a heat gain from April to the end of September (Fig. 5a). During autumn, the strong heat losses, induced by cold northerly wind events (Horton et al., 1997), weaken the stratification and induce mixing until depths around 40-50 m (Fig. 5b). The following northerly wind/heat loss events in winter further favor the deepening of the mixed layer, with the maximum depth ranging between 90 and 180 m in February/March. After March, the sea gains heat, restratifying the surface layer, and the MLD abruptly decreases. The seasonal pattern of modeled heat flux and mixed layer is in agreement with the climatology of the heat storage rates reported by D'Ortenzio et al. (2005) and Houpert et al. (2015). The Rhodes Gyre area displays a minimum winter temperature smaller than 16.5 °C in the Levantine Basin (Fig. S5a).

A strong wintry interannual variability of surface heat flux, as well as of wind stress magnitude and MLD, is clearly visible (Fig. 5 and S6, Table S1). Winters 2014-15, 2016-17, 2018-19 and 2019-20 are characterized by a winter mean heat loss higher than the seven year winter average, i.e. 130 W m^{-2} (Table S1, Fig. S6), and with mean winter mixed layer depth close to or higher than the seven year mean mixed layer of 68 m (Table S1). Cold winters (2014-15, 2018-19 and 2019-20) are also marked by strong winter wind stresses, except for 2016-17 characterized by the highest winter heat loss (Fig. S6). Among the mild winters, winter 2013-14 presents both a strong positive winter heat flux anomaly and a strong negative winter wind stress anomaly, as a consequence of the absence of cold winds from January onwards, leading to the shallowest mixed layers (Table S1). Negative anomalies of temperature are generally visible over the ML in winter and in subsurface during the stratification period for years of high winter heat losses (2014-15, 2016-17, 2018-19 and 2019-20, Fig. 5c). These anomalies extend below the subsurface for years 2014-15 and 2016-17 marked by deep winter mixing.

3.3 Variability of the pelagic planktonic ecosystem

Figure 6 presents the time series of vertical profiles of nutrients, phytoplankton, zooplankton and dissolved organic carbon concentrations, spatially averaged over the Rhodes Gyre area. We display both nitrate and phosphate due to their role of limitation on primary production in this region (Moutin and Raimbault, 2002).

During fall, nutrient concentrations gradually increase in the surface layer with the weakening of the stratification and the gradual rise of the nutricline (defined here as isoline 1 mmol N m^{-3} for nitracline and 0.05 mmol P m^{-3} for phosphacline) up to the surface (Fig. 6a, 6b and S7) induced by the intensification of the cyclonic circulation. As for the DOC, it starts decreasing gradually in mid-fall with the weakening of the stratification (Fig. 6e and S7).

10

https://doi.org/10.5194/bg-2022-216
Preprint. Discussion started: 21 November 2022

During winter, surface phytoplankton concentration starts to increase when mixed layer deepening intensifies and persistently reaches the nutriclines (Fig. 6a-c and S7a-d). The Rhodes Gyre area is enriched in nutrients at the surface (Fig. S5c) and is characterized by surface maximum chlorophyll concentrations over the Levantine Sea (Fig. S5b). The zooplankton concentration generally begins to increase after the onset of the phytoplankton accumulation in winter (Fig. 6d and S7e). The DOC concentration further decreases during the winter mixing period, from January to March (Fig. 6e and S7f). Increases in plankton and DOC concentrations under the surface layer (0-150 m) are clearly visible during that period (Fig. 6). The maximum surface concentration of organic carbon for phytoplankton reaches values higher than 0.5 mmol C m^{-3} between February and March (Fig. 6c, Table S1). Zooplankton concentration reaches its maximum (1-1.5 mmol C m^{-3}) near the surface in March-April (Fig. 6d). Phytoplankton accumulation stops at the surface when it becomes depleted in phosphate, the surface nitrate concentration ranging between 0.3 and 1 mmol N m^{-3}, in agreement with the observations of Yilmaz and Tugrul (1998) (Fig. 6a-c). Then, the deep chlorophyll maximum (DCM, green dotted line in Fig. 6c) forms. The DOC concentration progressively increases during spring (Fig. 6e).

During summer, the depletion in nutrients increases and deepens: phosphate and nitrate concentrations in the first 150 m are lower than 0.01 mmol P m^{-3} and 0.1 mmol N m^{-3}, respectively (Fig. 6a and 6b). The summer averaged nitracline and phosphacline are localized at 131 m and 144 m, respectively. The averaged DCM for all summer periods is at a mean depth of 128 m with magnitudes between 0.2 and 0.3 mg Chl m^{-3} (Fig. 6c). One should notice that the depth of DCM coincides with the depth of deep carbon maximum. Throughout the summer, the biomass of phytoplankton decreases. The decline of phytoplankton at the end of summer induces a zooplankton decrease (Fig. 6d). On the contrary, DOC accumulates due to stratification and reaches its maximum ranging from 52 to 55 mmol C m^{-3} in early August (Fig. 6e).

Interannual variability of nutrient concentrations and nutricline depths is strong during the mixing period when nutrients are injected into the surface layer (Fig. 6a and 6b, S7). During the cold winters of 2014-15, 2016-17, 2018-19 and 2019-20, the mixed layer reaches the nutriclines over a larger area (not shown) and period, allowing higher nutrient supplies into the surface layer (Table 1). Surface phytoplankton concentrations reach values higher than 1.5 mmol C m^{-3} and 0.3 mg Chl m^{-3} for those winters, whereas they don't exceed 1 mmol C m^{-3} and 0.23 mg Chl m^{-3} for the other winters (Table S1). Regarding zooplankton, the spring surface concentration is minimal during the mild year 2013-14 and maximum during the cold years 2016-17, 2018-19 and 2019-20 (Fig. 6d). High concentrations are also visible along the DCM layer for those years, as well as in 2018. DOC concentrations show similar interannual variability as zooplankton (Fig. 6e).

3.4 Organic carbon inventory and fluxes

Figures 7 and 8 represent, respectively in the surface (0 – 150 m) and intermediate (150 - 400 m) layers of the Rhodes Gyre area, the time series of the variation of the organic carbon inventory, of biogeochemical fluxes and of vertical and horizontal exchanges at the limits of the two boxes.

The inventory of organic carbon is minimum in January and maximum in June/July (Fig. 7a). The modeled gross primary production (GPP) generally follows the cycle of the solar insolation (not shown) with minimum values in December and maximum values at the end of June. A secondary peak is visible between February and April (Fig. 7b). The community respiration (CR) follows a similar pattern to the GPP with a temporal shift of a few weeks. The resulting net community production (NCP, corresponding to GPP minus CR) shows a peak

https://doi.org/10.5194/bg-2022-216
Preprint. Discussion started: 21 November 2022

value in February/March, during the secondary peak in the GPP, and negative values from August to January (Fig. 7c), indicating that the region is autotrophic from January to April and heterotrophic for the rest of the year.

The physical transport of organic carbon (POC plus DOC), by lateral and vertical mixing and advection, at the limits of the Rhodes Gyre area is negative almost all year round, and especially during the winter mixing period, which indicates an export of organic carbon from the surface layer (Fig. 7d). Winter export is mainly dominated by vertical downward fluxes, which concern both particulate and dissolved forms (Fig. 7e). Lateral export is more important for POC, with values exceeding 10 mmol C m^{-2} d^{-1} over several months for some summer/fall, when the DOC lateral export shows little variation along the period (Fig. 7f). The vertical export of total OC is reduced from spring onwards and becomes low (< 10 mmol C m^{-2} d^{-1}) in summer and autumn, when DOC can be injected into the surface layer.

The seasonal cycle of the organic carbon inventory in the intermediate layer is generally marked by a first peak during the winter mixing periods and a second peak in summer (Fig. 8a). The OC lateral exchange flux is negative from January to September, indicating a divergence of organic carbon from the Rhodes Gyre to the surrounding regions (Fig. 8b). During fall, it shows small inputs of organic carbon in the Rhodes Gyre. The vertical exchange flux (net difference between vertical fluxes at 150 m and vertical fluxes at 400 m), representing a net gain for the intermediate layer, generally shows an opposite sign to the lateral flux. The total (lateral plus vertical) OC transport (not shown) follows a similar pattern to the vertical flux variations, as vertical exchange flux dominates the lateral one. Finally, OC consumption shows maximum values during winter mixing periods, when heterotrophic respiration follows the downward input of surface OC (Fig. 8c). A secondary peak of OC respiration is visible in fall when the maximum POC concentration is the deepest.

In the surface layer, GPP shows interannual variability characterized by higher peak values during the restratification periods at the end of winter, for years 2014-15, 2016-17, 2018-19 and 2019-20 (Fig 7b) marked by strong winter mixing (Fig. 5b). Interannual variability of the seasonal cycle is less pronounced for CR, showing higher peaks following the late winter phytoplankton blooms for the same years (Fig. 7b). As a result, interannual variability of NCP is then linked with the variability of GPP, with higher winter NCP maxima reaching 40 mmol C m^{-2} d^{-1} for the strong mixing winters (Fig. 7c). The model results show that vertical export of POC and DOC at 150 m displays strong interannual variability during the winter mixing period with total OC export reaching 36 mmol C m^{-2} d^{-1} during severe winter years, and remaining lower than 10 mmol C m^{-2} d^{-1} during mild winter years for the surface layer (Fig. 7e).

Interannual variability can also be discerned in the intermediate layer (Fig. 8). Lateral flux is characterized by higher negative peaks during cold winters: the maximum lateral export exceeds 10 mmol C m^{-2} d^{-1} for cold years while it is limited to 3 mmol C m^{-2} d^{-1} during mild winters (Fig. 8b). OC consumption in February-March is more pronounced during cold years ranging between 5 and 8 mmol C m^{-2} d^{-1} compared to mild years, when it is limited to 2 mmol C m^{-2} d^{-1} (Fig. 8c).

3.5 Annual budget of organic carbon

Figure 9 presents the annual budget of organic carbon for the surface and intermediate layers of the Rhodes Gyre area, averaged over the seven year period (December 2013-December 2020), and Table 1 provides the terms of the budget for each year.

The model results show that, over the seven studied years, the annual biogeochemical flux (NCP) in the surface layer is positive (31.2 ± 6.9 g C m^{-2} $year^{-1}$) and more than three times higher than the OC consumption in the intermediate layer (-8.5 ± 3.1 g C m^{-2} $year^{-1}$) (Fig. 9). The annual downward export amounts to 16.8 ± 6.2 g C m^{-2} $year^{-1}$ and takes place under the form of POC and DOC (11.9 ± 3.4 versus 4.9 ± 2.8 g C m^{-2} $year^{-1}$, Table 1). The Rhodes Gyre appears as a source of organic carbon for the surface layer of the surrounding region (14.1 ± 2.1 g C m^{-2} $year^{-1}$). Then, we found that 54% of OC imported into the intermediate layer is locally remineralized into inorganic carbon (8.5 ± 3.1 g C m^{-2} $year^{-1}$), the remaining is mostly exported laterally to the surrounding area (7.5 ± 2.8 g C m^{-2} $year^{-1}$). The organic carbon export towards the deeper layer is 16 times weaker (1.01± 0.5 g C m^{-2} $year^{-1}$) than the downward export from the surface layer. The variation in organic carbon inventory remains low in the surface and intermediate layers (0.44 and 0.09 g C m^{-2} $year^{-1}$, respectively), indicating a quasi-balance between biogeochemical production and physical transfers over the seven year period.

The biogeochemical fluxes, i.e. PP, CR and NCP, all show an annual mean stronger than the seven year average during the cold winter years 2016-17, 2018-19 and 2019-20 (Table 1). However, the magnitude of PP and CR appears to be higher for the mild winter year 2017-18 compared to the cold winter year 2014-15. Regarding the physical transfer, we found that particulate and dissolved OC downward export show clearly stronger annual mean during all cold winter years (2014-15, 2016-17, 2018-19 and 2019-20). The lateral export in the surface is generally also stronger during cold years, except during the year 2016-17 which shows the lowest lateral OC export. Nevertheless, this latter year shows both the highest OC downward export from the surface and the highest lateral export in the intermediate layer towards the surrounding region, suggesting that lateral export is deepened during this very cold winter (Fig. 5c).

4 Discussion

This study describes the temporal evolution of the plankton (phytoplankton and zooplankton) ecosystem and particulate and dissolved organic carbon fluxes in the Rhodes Gyre for the period from December 2013 to April 2021. To our knowledge, it is the first attempt to quantify, based on a 3D coupled biogeochemical-physical model, an organic carbon budget in the Rhodes Gyre, the main formation site of LIW.

In this section, first we discuss the robustness of the model results. Then, we investigate the interannual variability of phytoplankton growth, OC export and NCP in the Rhodes Gyre area. The interannual variability of those fluxes could be driven by various factors: local atmospheric forcing (heat flux, wind stress, evaporation minus precipitation), as well as more or less distant drivers, such as the reversal of the North Ionian Gyre (Ozer et al., 2022). In this study, we focus on the impact of winter mixing.

4.1 Model skill assessment

The comparisons of model results with the available data sets, presented in Sect. 3.1, show an overall good agreement in the seasonal dynamics and vertical distribution of chlorophyll, nutrients and dissolved oxygen in the Levantine Sea. We notice however an underestimation in the magnitude of the modeled maximum chlorophyll and dissolved oxygen concentration when comparing with both the BGC-Argo float and cruise data. One should notice that ocean color and in situ data remain scarce in the Levantine Sea, and especially in the Rhodes Gyre (D'Ortenzio et al., 2021) making the evaluation exercise difficult and partial. Additional in situ observations in the study area are required to further refine the biogeochemical model results. Comparisons with

https://doi.org/10.5194/bg-2022-216
Preprint. Discussion started: 21 November 2022

complementary biological and biogeochemical observations carried out during the PERLE cruises whose analyses are in progress will be used in near future studies to continue the evaluation.

Here, we complete the direct comparisons with in situ and satellite observations comparisons from the literature. In the model result, DOC concentrations show a rapid decrease with depth from values ranging between 45 and 64 mmol C m^{-3} in the surface layer to values around 40 mmol C m^{-3} below 300 m depth (Fig. 6e). These results are in agreement with what was reported in previous observational studies in the Levantine Sea (Krom et al., 2005; Santinelli et al., 2010; Pujo-Pay et al., 2011; Martinez Perez et al., 2017). The surface values fall in the lower range of observations (41-100 mmol C m^{-3}), which could be partly explained by the locations of the observations, mostly outside the Rhodes Gyre in more stratified and less productive regions. The model DOC concentrations exhibit a clear seasonal cycle in the surface layer, with maximum values at the end of summer and low values during winter mixing periods when surface waters are mixed with deeper DOC-poorer waters and DOC is transported towards intermediate depths. This variability is in line with the few observational studies documenting the seasonal cycle in the Ligurian and southern Adriatic seas characterized by strong winter mixing (Avril et al., 2002; Santinelli et al., 2013).

Regarding the organic carbon biological fluxes, the seven year averaged annual NPP that amounts to 115 ± 15 g C m^{-2} year^{-1} falls in the range of the previous annual estimates based on both the satellite ocean color data for the eastern Mediterranean Basin (EM) or more specifically for the Rhodes Gyre (RG) (87 g C m^{-2} year^{-1} in EM by Antoine et al. (1995); 121 ± 5 g C m^{-2} year^{-1} in EM by Bosc et al. (2004); ~75 g C m^{-2} year^{-1} in EM by Uitz et al. (2012)), and on 1D (97 ± 5 g C m^{-2} year^{-1} in RG by Napolitano et al. (2000)) and 3D modeling (76 ± 5 g C m^{-2} year^{-1} by Lazzari et al. (2012), 140-180 g C m^{-2} year^{-1} in RG by Kalaroni et al. (2020), ~130 g C m^{-2} year^{-1} in RG by Cossarini et al. (2021)) studies. The higher winter NPP values in the Rhodes Gyre area compared to the surrounding Levantine Basin (Fig. S5d) are in agreement with the findings of Vidussi et al. (2001).

The mean annual POC export at 150 m depth is estimated in the model at 11.9 ± 3.4 g C m^{-2} year^{-1}. It is in the range of estimates deduced from sediment traps measurements: it is lower than the annual estimates of POC flux derived at 100 m depth from deep (1000-1400 m) sediment traps in the Gulf of Lion and Ionian Sea, of 23.3 and 15.7 g C m^{-2} year^{-1}, respectively (Gogou et al., 2014); it is higher than those deduced from sediment trap measurements at 150 m of 3.3 and 2.6 g C m^{-2} year^{-1} in the southern Adriatic and Ionian seas, respectively (Boldrin et al., 2002). The June monthly POC export from the model is twice as high as the POC export reported for the Rhodes Gyre for May-June 1996 by Moutin and Raimbault (2002) (43 versus 21 mg C m^{-2} d^{-1}). We found higher POC export than other modeling studies (1 g C m^{-2} year^{-1} at 400 m vs. < 0.1 g C m^{-2} year^{-1} at 500 m by Cossarini et al. (2021); 2.4 g C m^{-2} year^{-1} at 100 m in the eastern basin by Guyennon et al. (2015))

The mean fraction of NPP exported from the surface under the particulate form represents 10 % of the total NPP in the model. This is in the range of what was estimated for the measured carbon export by Buesseler (1998) for the global ocean (2-20%), similar to the estimates of 11% for the western and eastern Mediterranean sites by Gogou et al. (2014) and to the estimates of 9 % by Moutin and Raimbault (2002) for the Rhodes Gyre.

Our estimate of the annual DOC export at 150 m depth amounts to 4.9 ± 2.8 g C m^{-2} year^{-1}. It shows a high interannual variability, which is discussed in Sect. 4.3. It is smaller than the annual DOC flux estimated at 100 m at 12 g C m^{-2} yr^{-1} in the Ligurian Sea by Avril (2002) and at 50 m depth at 15.4 g C m^{-2} yr^{-1} in the southern Adriatic Sea by Santinelli et al. (2013), both sites being characterized by strong winter mixing. On the contrary,

https://doi.org/10.5194/bg-2022-216
Preprint. Discussion started: 21 November 2022

our estimate is greater than the DOC flux at 50 m of 3.2 g C m^{-2} yr^{-1} estimated in the stratified Tyrrhenian Sea by Santinelli et al. (2013).

The modeled organic carbon fluxes appear to be in the order of magnitude of those deduced from observations, although we are conscious that the comparisons between both estimates are not straightforward, due notably to the definition of the processes (Ducklow and Doney, 2003; Di Biagio et al., 2022), the composition of OC considered (Gali et al., 2022) and the difference in time and locations.

4.2 Influence of winter mixing on phytoplankton growth

The model results display a similar general seasonal cycle of phytoplankton net growth from years 2013-14 to 2019-20 in the Rhodes Gyre area, depicted in Fig. 6 and S7. The intensification of the cyclonic circulation in fall favors the shallowing of the nutriclines. Then, vertical mixing events induce the injection of nutrients near the surface at the end of November/early December, leading to an increase in nutrient concentrations near the surface (Fig S5c). On average over the seven studied years, phytoplankton concentration at the surface is increasing progressively from the end of November/early December until mid-February/early March and then decreases following the depletion of nutrients near the surface. A DCM develops and deepens when the water column becomes permanently stratified until the end of summer. On average, the period of phytoplankton accumulation at the surface is concomitant with the global period of vertical mixing. This is in agreement with the modeling results for the whole Levantine Sea by Lazzari et al. (2012) and the satellite and BGC-Argo observations in the Rhodes Gyre reported by Lavigne et al. (2013), Mignot el al. (2014) and D'Ortenzio et al. (2021).

Although this similar general seasonal pattern of ecosystem dynamics can be found for all the studied years, the model results exhibit pronounced interannual variability over the period in terms of magnitude and timing of nutrient injection into the surface and phytoplankton growth. Our model results show that during cold winters (years 2014-15, 2016-17, 2018-19 and 2019-20), deeper mixing leads to higher nutrient supply into the euphotic layer. Nutrient injection is more than twice as high during severe winters compared to mild winters (Table 1). We explore over the seven years the relationship between this term and two indicators of winter severity, on the one hand the winter heat loss and on the other hand the winter mean MLD. In both cases, the correlation is significant but slightly higher for heat loss, which has the advantage of being readily available from meteorological analyses. Considering that the year 2013-14 is characterized by a particularly warm winter, we also established the relationship without this year. Figure 10a shows the relationship between winter heat loss and vertical phosphate injection. We found a significant correlation between nutrient injection and mean winter HL (heat loss) or mean winter MLD (higher than 0.85). This result is in line with previous observational (Ediger and Yilmaz, 1996; Yilmaz and Tugrul, 1998) and modeling (Napolitano et al, 2000) studies in the Rhodes Gyre.

Then the model shows that strong nutrient supply into the euphotic layer favors more intense phytoplanktonic blooms. During cold winters, the spatially averaged value of maximum surface chlorophyll is higher than 0.3 mg Chl m^{-3}, whereas it is 0.15 mg Chl m^{-3} during the very mild winter 2013-14 (Table S1, Fig. 6c). The model winter and spring PP (not shown) are higher during cold winter years, leading to higher annual PP, except for the year 2014-15. The model annual NPP is significantly correlated with mean winter HL ($R > 0.86$, Fig. 10e) and MLD. This is in agreement with several previous studies based on in situ measurements (Ediger and Yilmaz, 1996), satellite data (D'Ortenzio et al., 2003) and modeling (Napolitano et al., 2000; Pedrosa-Pamies et al., 2016). The low annual PP during the year 2014-15, could be driven by a combination of various factors: (i) an unfavorable initial state following the particularly mild year 2013-14, (ii) the short duration of intense mixing events leading to PP close to the seven year mean value in winter and spring (not shown), and (iii) low PP in summer, marked by a negative temperature anomaly and low solar radiation (not shown).

On the other hand, the model PP relies at 30% on the uptake of nitrate, and at 70% on the uptake of ammonium (not shown). The former is significantly correlated with HL (R> 0.88, Fig. 10g) and MLD, whereas no correlation can be found between the latter and HL (R< 0.69, Fig. 10h) or winter mixing. Thus the intensity of mixing that determines the amount of new deep nutrient available for primary production doesn't strongly impact recycled production. Other driving factors such as trends in temperature and nutricline depth as observed in the southeastern Levantine Basin (Ozer et al., 2022) that we don't address in this study could also influence the variability of annual PP.

Regarding the timing of phytoplankton concentration and growth, our results also highlight net interannual variability linked to intraseasonal atmospheric forcing. The evolution of modeled vertical mixing, nutrient and chlorophyll for 2013-14, 2014-15, 2015-16 years, shown in Fig. 11, allows specifying the interplay between vertical mixing and phytoplankton growth. The model shows a common progressive increase of surface chlorophyll and NPP when the mixed layer locally reaches the nutriclines in December. A very rapid increase (< one day) of surface concentrations of nutrients occurs in response to the acceleration of the deepening of the ML. Then, peaks of surface chlorophyll and NPP rapidly succeed to those synchronous peaks of MLD and nutrients. When the MLD exceeds the depth of the euphotic layer, as in February 2015 or late January 2016, surface chlorophyll decreases, while depth-integrated chlorophyll (not shown) and NPP decrease or remain stable, temporarily and locally, due to dilution of phytoplankton cells over the ML and light limitation for phytoplankton growth. As an example, Fig. S8 shows a low chlorophyll concentration on 20 February 2015 in the core of the Rhodes Gyre where vertical mixing is the most intense, with higher concentrations in the border of the gyre (panels (a) and (c)). Modeled surface chlorophyll averaged over the Rhodes Gyre area is then maximum 12 days later, on 4 March 2015, when it reaches higher concentrations in the center of the gyre as soon as the water column restratified (Fig. S8b-d). This modeled spatial variability is in agreement with the study of Ediger et al. (2005) who reported higher PP and biomass at the periphery of the gyre than in its homogenized center, based on observations collected in March 1992 when a deep convection event occurred. With regard to the date of the maximum surface chlorophyll no clear link with winter severity can be established. The former is instead related to the timing and history of wind events favoring the deepening of the ML, submitted to high interannual variability. For example, the dates of maximum MLD and chlorophyll are in March during both the mild winter 2013-14 and the severe winter 2014-15 (Table S1).

In the Rhodes Gyre, the episodes of strong surface phytoplankton growth, as well as of its interruption due to vertical mixing deeper than the base of the euphotic zone, remain short. They are markedly shorter than in the other Mediterranean regions of deep water formation, especially compared to the northwestern Mediterranean region where deep mixing can last for two months during intense convection years (i.e. 2004-05, 2005-06, 2012-13; Bernardello et al., 2012; Ulses et al., 2016; Mayot et al., 2017; Kessouri et al., 2018).

https://doi.org/10.5194/bg-2022-216
Preprint. Discussion started: 21 November 2022

Biogeosciences Discussions

4.3 Influence of winter mixing on organic carbon export

Several processes of deep organic matter export have been highlighted in different regions of the globe, in particular the gravitational biological pump related to the fall of large phytoplankton cells (Sanders et al., 2014), the eddy-driven subduction pump occurring at submesoscale (1-10 km) (Omand et al., 2015) able to export non sinking particles and dissolved organic carbon, and the mixed layer pump related to the detrainment of organic matter at the transition between deep and shallow mixed layers occurring at seasonal (Dall'Olmo et al., 2016), intraseasonal (Lacour et al., 2019) and daily time scales (Gardner et al., 1995). All of these processes are particularly effective at high latitudes that favor the development of large phytoplankton cells, deep vertical mixing, and instabilities that arise from restratification and generate submesoscale eddies. These physical factors are also found in the deep convection zones of the Mediterranean. Kessouri et al. (2018) showed in the dense water formation region of the northwestern Mediterranean that the export fluxes of POC and DOC at 150 m during convective periods represent, respectively, 50 and 60%, of the annual export and that this export is 5 times larger than in the neighboring Algerian Basin. Boldrin et al. (2002) showed that in the southern Adriatic vertical mixing during convection supplying inorganic nutrients in the upper layers from the deep, is the dominant process, increasing primary production and downward fluxes of particulate matter in early spring. Santinelli et al. (2013) found in the southern Adriatic that DOC accumulated during high stratification periods was exported in winter by deep convection. More precisely, convection intermittencies favor the export: Bernardello et al. (2012) showed that the frequency of gales during the bloom period was a determining factor in the interannual variability of export in the deep convection region of the northwestern Mediterranean. Kessouri et al. (2018) also showed in this region the mechanism of mixed layer pump during winter with an alternation of periods of restratification, that favors phytoplankton growth, and of vertical mixing, that entrains a fraction of the new biomass under the euphotic layer. The processes in the case of intermediate convection of the Rhodes Gyre have similarities to those of deep convection but the time scales of production and export are shorter. The depth of mixing is not sufficient to persistently inhibit production, which allows for more continuous export throughout the winter period. Intermittency of convection is thus less necessary to trigger the export than for deep convection.

One issue is to determine to what extent winter impacts, through the intensity of convection, (i) locally in the Rhodes Gyre, the organic carbon budget through the carbon export terms under the euphotic layer and the activity of the intermediate layers ecosystem, and (ii) remotely its redistribution towards the Levantine Basin. Figures 10b,c,d show the relationship between winter heat loss, and three annually integrated fluxes: vertical export of organic carbon at 150 m, respiration and the lateral flux of organic carbon from the intermediate layer (150-400 m) exported from the Rhodes Gyre to the Levantine Basin. The correlation for the seven years data set is greater than 0.86 (p-value <0.02) for all variables and increases to more than 0.9 (p-value <0.005) if 2013-14, the warmest winter, is removed indicating that it is an atypical year. Compared to the linear regression inferred from the other six years (red line), 2013-14 is above the regression line, meaning stronger vertical and horizontal fluxes than predicted by the regression (values approaching 0 or even negative). Unlike the other years, the seasonal cycle of export at 150 m indeed shows no clear signal in winter (Fig. 7e), and in the surface layer GPP also shows no notable peak in winter and spring (Fig. 7b). For this exceptionally warm year, the fluxes are therefore not driven by winter conditions. It is likely that the fluxes of the year 2013-14 which are close but weaker to those of the second warmest year (2017-18), are close to be minimum values for the Rhodes Gyre.

Regarding the annual lateral OC flux from the Rhodes Gyre to the Levantine Basin in the intermediate layer clearly related to winter severity (Fig. 10c). It shows a correlation of 0.97 (p-value <) with OC vertical export at 150 m allowing to identify the responsibility of physical processes of LIW formation. A parallel can be drawn with salinity, whose high values mark the intermediate waters of the entire Mediterranean basin. Salinity increases in the surface layer throughout summer and fall through evaporation (Estournel et al., 2021). Convection resulting from cooling/densification of the surface waters in winter and favored by weak stratification linked to the presence of the cyclonic gyre then transfers salt to the whole winter MLD. Waters of the Rhodes Gyre, which are much denser than surrounding waters, are then subducted along isopycnals towards the Levantine Basin, as observed by Taillandier et al. (2022), forming the salty Levantine Intermediate Water (LIW) that further disperses towards all the Mediterranean Sea until Gibraltar. Figure 12 shows a vertical section of phytoplankton on 27 March 2015, six days after the last cold event of the season during which the mixed layer reaches about 200 m in the center of the gyre (latitude: 34.9°N). The stratification of the first 30 m that establishes after the wind stops allows the growth of phytoplankton biomass, which appears decoupled from deeper phytoplankton. Tongues of phytoplankton sink along isopycnals on either side of the front bordering the gyre. On the south side (34.2-34.4°N), two structures approximately follow isopycnals 28.75 and 29 kg m^{-3} and are separated by a phytoplankton-poor, nutrient-rich (not shown) ascending structure along isopycnal 28.9 kg m^{-3}. The presence of ascending structures could be the cause of the high surface phytoplankton concentrations in the frontal zone (around 34.4-34.5 °N). On the northern side of the gyre (~35.4°N), phytoplankton biomass is exported between isopycnals 29 and 29.1 kg m^{-3}. The along isopycnals up- and downward interleavings of nutrient/phytoplankton are similar to those observed by glider along the front surrounding the northwestern Mediterranean deep convection zone (Niewiadomska et al., 2008; Bosse et al., 2021). These authors highlight the secondary vertical circulation associated with the front and specifically the role of down-front winds producing cross front advection of dense water. This process triggers frontal instabilities resulting in water overturning along isopycnals within typically 1-5 km cross-frontal slanted cells with subduction on the dense side of the front and upwelling along the frontal interface (Thomas and Lee, 2005). Our model indicates that such vertical circulation is a major mechanism after each convection event to export organic carbon from the Rhodes Gyre below the euphotic layer and likely to bring up nutrients that extends the bloom duration. The respective role of wind and surface heat fluxes in triggering front instabilities will need to be investigated more precisely.

Taillandier et al. (2022) indicated that the volume of dense water in the Rhodes Gyre region returns to its pre-convection level in two to three months which gives an estimate of the time scale of lateral export that is in agreement with the model's assessment showing lateral export of organic carbon from the intermediate layer of the Rhodes Gyre that becomes low from April onwards (Fig. 8b). Regarding organic carbon, these physical processes (convection/subduction) are modulated by biogeochemical processes, for example, consumption by respiration which competes with physical export. The regression between vertical and lateral export over the seven years indicates that 45% of organic carbon exported below 150 m depth is exported to the Levantine Basin while 50% is consumed by respiration inside the Rhodes Gyre intermediate layer.

4.4 Influence of winter mixing on carbon sequestration

The modeled NCP in the surface layer (Fig. 7c) indicates that the planktonic ecosystem has an autotrophic metabolism from January to August, with maximum values between 30 and 60 mmol C m^{-2} d^{-1} during the phytoplankton bloom, and an heterotrophic metabolism from September to December. This is consistent with the study by Wimart-Rousseau et al. (2021) based on cruise observations of the carbonate system at three different seasons, and the biogeochemical reanalysis by Cossarini et al. (2021). At the annual scale, the planktonic ecosystem in the Rhodes Gyre acts as a sink of atmospheric CO_2 with an estimate of mean NCP at 31.2 ± 6.9 g C m^{-2} yr^{-1}. This OC net biological production (DIC consumption) is almost balanced by both the OC lateral and vertical transports with a quasi-evenly distribution (14.1 ± 2.1 and 16.8 ± 6.2 g C m^{-2} yr^{-1}, respectively). The OC exported towards the intermediate layer is further respired or laterally exported by subduction towards the surrounding Levantine Basin, mostly during the dispersion of the newly formed LIW. We estimate that 1.0 ± 0.5 g C m^{-2} yr^{-1}, i.e. 1% and 3% of the NPP and NCP, respectively, is then transferred towards the deeper depths. On the other hand, OC exported in the LIW flowing towards the surrounding Levantine, Aegean and Ionian seas (Estournel et al., 2021) will also be affected by respiration, sinking, advection and mixing processes along its path.

High interannual variability of annual NCP (SD of 22%) in the Rhodes Gyre appears to be primarily linked to the intensity of winter atmospheric HL and vertical mixing (significant correlation > 0.88 between annual NCP and winter HL, Fig. 10f), which indicates an enhanced autotrophic metabolism during cold years.

In this study, we describe only partially the cycle of DIC through its biological consumption. Air-sea flux and transport terms of the inorganic form of carbon are not considered here. This limits the determination of the role of the Rhodes Gyre relative to atmospheric CO_2 uptake and of the influence of winter mixing intensity on this uptake. Previous studies reported that a significant amount of OC exported below the euphotic layer could be reinjected back under organic or remineralized form during the following winters in convection regions (Oschlies et al., 2004; Körtzinger et al., 2008; Palevsky and Quay, 2017). Over the study period, one can notice the succession of two convective years, 2018-19 and 2019-20, however the second year does not display particularly low net OC downward export compared to the other cold years (Fig. 10b). On the other hand, observational (Hood and Merlivat, 2001; Copin-Montégut et al., 2004; Merlivat et al., 2018) and modeling (Mémery et al., 2002; Ulses et al., submitted) studies in the NW Mediterranean deep convection region showed that CO_2 air-sea fluxes are reduced during periods of intense winter mixing. In their modeling study on the budget of DIC in the NW Mediterranean Sea, Ulses et al. (in prep.) estimated that large amounts of DIC are vertically supplied into the euphotic layer during convection, and then partly laterally exported towards the general circulation. The impact of winter mixing on total carbon sequestration is thus difficult to establish and requires the description of the dynamics of the carbonate system in the model that will be investigated in a near-future study.

Based on a 1D coupled model combined with satellite data, D'Ortenzio et al. (2008) and Taillandier et al. (2012), reported a CO_2 air-sea flux between -1.5 and -0.5 mol C m^{-2} yr^{-1}, in the Rhodes Gyre and the whole Levantine Sea acting thus as a source for the atmosphere. Cossarini et al. (2021) modeled the temporal evolution of CO_2 air-sea fluxes from 1999 to 2019. They found that the Rhodes Gyre is a small sink of atmospheric CO_2 (< 0.25 mol C m^{-2} yr^{-1}), whereas the surrounding Levantine Basin is a source for the atmosphere. Besides, they reported an increasing absorption of atmospheric CO_2 in both the eastern and western Mediterranean Sea,

https://doi.org/10.5194/bg-2022-216
Preprint. Discussion started: 21 November 2022

Biogeosciences Discussions

leading to a change in the sign of air-sea exchanges averaged over the eastern Mediterranean, and a switch from source to sink, at the end of the period (2019), in response to the increase of atmospheric CO_2. Hassoun et al. (2019) and Wimart-Rousseau et al. (2021) derived an increasing trend in inorganic carbon content in the coastal and open-sea Levantine Basin, based on observations. The predictions for the carbon cycle in the Mediterranean Sea over the 21st century by Solidoro et al. (2022) and Reale et al. (2022) showed a further increase in atmospheric CO_2 absorption, which, together with the increasing temperature and stratification (Somot et al., 2006; Soto-Navarro et al. 2020), leads to an increase in carbon content.

5 Conclusion

In this study we have used a 3D coupled hydrodynamic – biogeochemical model to investigate the pelagic ecosystem functioning and estimate a budget of organic carbon in the Rhodes Gyre, over the period of 2013-2020, marked by the alternation of cold and mild winter years. The assessment of the model results based on satellite, cruise, and BGC-Argo float observations in the Levantine Basin demonstrates that the model was able to reproduce reasonably well the main seasonal and spatial evolution of physical and biogeochemical observed variables.

The model confirms that the intensity of winter surface heat loss and vertical mixing events significantly influences the magnitude of nutrient supplies into the euphotic layer and of surface phytoplankton growth. The development of phytoplankton at the surface is always concomitant with the winter mixing period. It is characterized by a first phase of progressive growth with the deepening of the mixed layer, and a second phase consisting of alternating short periods (< 2 weeks) of vertical mixing and of phytoplankton growth episodes during temporary restratification. This second phase only occurs during severe winters due to the dilution of phytoplankton biomass over the mixed layer and the reduction of light availability. A spatial variability is also depicted in the gyre during the mixing period. Under prolonged winter conditions, the characteristics of the phytoplankton bloom are present at the periphery of the Rhodes Gyre, when vertical mixing is intense, and reappear in the center of the gyre at the restratification. At the end of the mixing period, a DCM forms and progressively deepens until mid-summer.

Our results show that the Rhodes Gyre is characterized by an alternation between phytoplankton growth and OC export from the upper layer, favored by vertical mixing episodes. OC is transported vertically towards intermediate depths and laterally towards the surrounding regions, partly by subduction during the dispersion of LIW. The annual downward OC export is strongly enhanced with the intensity of winter surface heat flux, with annual export 2 to 3 times higher during cold winter years compared to mild winter years. 50% of the organic carbon exported below 150 m depth in the Rhodes Gyre is remineralized at intermediate levels inside the gyre and 45% is exported towards the surrounding Levantine Basin. The Rhodes Gyre acts as a source of organic carbon for the surrounding areas.

The Rhodes Gyre is found to be an autotrophic ecosystem, with net community production in the surface layer accounting for 31.2 ± 6.9 g m^{-2} year^{-1}. Finally, our modeling study is constrained to the Rhodes Gyre and a seven year period. Its spatial and temporal extension could allow the examination of (i) the fate of the organic carbon produced in the Rhodes Gyre after its export to the Levantine Basin and to the other regions of the eastern Mediterranean Sea, as well as (ii) the influence of remote drivers on biological activity and physical processes in the Levantine Basin.

20

https://doi.org/10.5194/bg-2022-216
Preprint. Discussion started: 21 November 2022

Code availability

The SYMPHONIE model and the MATLAB codes used to process the model outputs are available from the authors on request.

Data availability

Data used to validate the model are available on different websites specified in the main text of the manuscript. These data and the model outputs are also available from the authors on request.

Competing interests

The authors declare that they have no conflict of interest.

Acknowledgments

This study is a contribution to the MerMex (Marine Ecosystem Response in the Mediterranean Experiment) project of the MISTRALS international program. The numerical simulations were performed using the SYMPHONIE model, developed by the SIROCCO group (https://sirocco.obs-mip.fr/, last access: 17 October 2022), and computed on the cluster of Laboratoire d'Aérologie and HPC resources from CALMIP grants (P1325, P09115 and P1331). We acknowledge the scientists and crews of the Flotte océanographique française (https://www.flotteoceanographique.fr/, last access: November 2022) who contributed to the cruises carried out in the framework of the PERLE project. The authors would like to acknowledge the National Council for Scientific Research of Lebanon (CNRS-L), Campus France, the University of Toulouse and LEGOS for granting a doctoral fellowship to Joëlle Habib. We thank Marta Álvarez (IEO, La Coruña) and collaborators for making available the CARIMED database to us. We also warmly thank Pierre Nabat from CNRM for providing the atmospheric deposition data.

References

Alkalay, R., Zlatkin, O., Katz, T., Herut, B., Halicz, L., Berman-Frank, I., and Weinstein, Y.: Carbon export and drivers in the southeastern Levantine Basin, Deep Sea Research Part II: Topical Studies in Oceanography, 171, 104 713, https://doi.org/10.1016/j.dsr2.2019.104713, 2020.

Álvarez, M., Velo, A., Tanhua, T., Key, R., Heuven, S. V., Español, I., Ieo, D. O., Coruña, A., and Marinas, I. D. I.: Carbon, tracer and ancillary data in the MEDSEA, CARIMED: an internally consistent data product for the Mediterranean Sea., Tech. Rep. 2019, Instituto Español de Oceanografía, 2019.655

Antoine, D., Morel, A., and Andre, J. M.: Algal pigment distribution and primary production in the eastern Mediterranean as derived from coastal zone color scanner observations, Journal of Geophysical Research, 100, https://doi.org/10.1029/95jc00466, 1995.

Argo: Argo float data and metadata from Global Data Assembly Centre (Argo GDAC), SEANOE, https://doi.org/https://doi.org/10.17882/42182, 2022.

Astraldi, M., Balopoulos, S., Candela, J., Font, J., Gacic, M., Gasparini, G. P., Manca, B., Theocharis, A., and Tintoré, J.: The role of straits and channels in understanding the characteristics of Mediterranean circulation, Progress in Oceanography, 44, 65–108, https://doi.org/10.1016/S0079-6611(99)00021-X, 1999.

Auger, P. A., Diaz, F., Ulses, C., Estournel, C., Neveux, J., Joux, F., Pujo-Pay, M., and Naudin, J. J.: Functioning of the planktonic ecosystem on the Gulf of Lions shelf (NW Mediterranean) during spring and its impact on the carbon deposition: A field data and 3-D modelling combined approach, Biogeosciences, 8, 3231–3261, https://doi.org/10.5194/bg-8-3231-2011, 2011.

Auger, P. A., Ulses, C., Estournel, C., Stemmann, L., Somot, S., and Diaz, F.: Interannual control of plankton communities by deep wintermixing and prey/predator interactions in the NW Mediterranean: Results from a 30-year 3D modeling study, Progress in Oceanography,124, 12–27, https://doi.org/10.1016/j.pocean.2014.04.004, 2014.

Avril, B.: DOC dynamics in the northwestern Mediterranean sea (DYFAMED site), Deep-Sea Research Part II: Topical Studies in Oceanography, 49, 2163–2182, https://doi.org/10.1016/S0967-0645(02)00033-4, 2002.670

Bernardello, R., Cardoso, J. G., Bahamon, N., Donis, D., Marinov, I., and Cruzado, A.: Factors controlling interannual variability of vertical organic matter export and phytoplankton bloom dynamics-a numerical case-study for the NW Mediterranean Sea, Biogeosciences, 9, 4233–4245, https://doi.org/10.5194/bg-9-4233-2012, 2012.

Bittig, H. C. and Körtzinger, A.: Tackling oxygen optode drift: Near-surface and in-air oxygen optode measurements on a float provide an accurate in situ reference, Journal of Atmospheric and Oceanic Technology, 32, 1536–1543, https://doi.org/10.1175/JTECH-D-14-00162.1, 2015

Bittig, H. C., Körtzinger, A., Neill, C., van Ooijen, E., Plant, J. N., Hahn, J., Johnson, K. S., Yang, B., and Emerson, S. R.: Oxygen optode sensors: Principle, characterization, calibration, and application in the ocean, Frontiers in Marine Science, 4, 1–25, https://doi.org/10.3389/fmars.2017.00429, 2018.

Boldrin, A., Miserocchi, S., Rabitti, S., Turchetto, M. M., Balboni, V., and Socal, G.: Particulate matter in the southern Adriatic and Ionian Sea: Characterisation and downward fluxes, Journal of Marine Systems, 33-34, 389–410, https://doi.org/10.1016/S0924-7963(02)00068-4,675,2002.

Bosc, E., Bricaud, A., and Antoine, D.: Seasonal and interannual variability in algal biomass and primary production inthe Mediterranean Sea, as derived from 4 years of SeaWiFS observations, Global Biogeochemical Cycles, 18,https://doi.org/10.1029/2003gb002034, 2004.

Bosse, A., Testor, P., Damien, P., Estournel, C., Marsaleix, P., Mortier, L., Prieur, L., and Taillandier, V.: Wind-forced submesoscale symmetric instability around deep convection in the northwestern mediterranean sea, Fluids, 6, 1–26, https://doi.org/10.3390/fluids6030123, 2021.

Brenner, S., Rozentraub, Z., Bishop, J., and Krom, M.: The mixed-layer/thermocline cycle of a persistent warm core eddy in the eastern Mediterranean, Dynamics of Atmospheres and Oceans, 15, 457–476, https://doi.org/10.1016/0377-0265(91)90028-E, 1991.

Buesseler, K. O.: The decoupling of production and particulate export in the surface ocean, Global Biogeochemical Cycles, 12, 297–310, https://doi.org/10.1029/97GB03366, 1998.

Copin-Montégut, C., Bégovic, M., and Merlivat, L.: Variability of the partial pressure of CO2 on diel to annual time scales in the Northwestern Mediterranean Sea, Marine Chemistry, 85, 169–189, https://doi.org/10.1016/j.marchem.2003.10.005, 2004.

Coppola, L., Prieur, L., Taupier-Letage, I., Estournel, C., Testor, P., Lefevre, D., Belamari, S., LeReste, S., and Taillandier, V.: Observation of oxygen ventilation into deep waters through targeted deployment of multiple

Argo-O2 floats in the north-western Mediterranean Sea in 2013, Journal of Geophysical Research: Oceans, 122, 6325–6341, https://doi.org/10.1002/2016JC012594, 2017.

Cornec, M., Laxenaire, R., Speich, S., and Claustre, H.: Impact of Mesoscale Eddies on Deep Chlorophyll Maxima, Geophysical Research Letters, 48, https://doi.org/10.1029/2021gl093470, 2021.

Cossarini, G., Feudale, L., Teruzzi, A., Bolzon, G., Coidessa, G., Solidoro, C., Di Biagio, V., Amadio, C., Lazzari, P., Brosich, A., and Salon, S.: High-Resolution Reanalysis of the Mediterranean Sea Biogeochemistry (1999–2019), Frontiers in Marine Science, 8, 1–21, https://doi.org/10.3389/fmars.2021.741486, 2021.

Dall'Olmo, G., Dingle, J., Polimene, L., Brewin, R. J., and Claustre, H.: Substantial energy input to the mesopelagic ecosystem from the seasonal mixed-layer pump, Nature Geoscience, 9, 820–823, https://doi.org/10.1038/ngeo2818, 2016.

Damien, P., Bosse, A., Testor, P., Marsaleix, P., and Estournel, C.: Modeling Postconvective Submesoscale Coherent Vortices in the North-western Mediterranean Sea, Journal of Geophysical Research: Oceans, 122, 9937–9961, https://doi.org/10.1002/2016JC012114, 2017.

Di Biagio, V., Salon, S., Feudale, L., and Cossarini, G.: Subsurface oxygen maximum in oligotrophic marine ecosystems: mapping the interaction between physical and biogeochemical processes, Biogeosciences, 2018, 1–33, https://doi.org/10.5194/bg-2022-70,2022

D'Ortenzio, F. and Ribera d'Alcalà, M.: On the trophic regimes of the Mediterranean Sea: a satellite analysis, Biogeosciences Discussions,5, 2959–2983, https://doi.org/10.5194/bgd-5-2959-2008, 2009.

D'Ortenzio, F., Ragni, M., Marullo, S., and Ribera d'Alcalà, M.: Did biological activity in the Ionian Sea change after the Eastern Mediterranean Transient? Results from the analysis of remote sensing observations, Journal of Geophysical Research: Oceans, 108,https://doi.org/10.1029/2002jc001556, 2003.

D'Ortenzio, F., Iudicone, D., de Boyer Montegut, C., Testor, P., Antoine, D., Marullo, S., Santoleri, R., and Madec, G.: Seasonal variability of the mixed layer depth in the Mediterranean Sea as derived from in situ profiles, Geophysical Research Letters, 32, 1–4, https://doi.org/10.1029/2005GL022463, 2005.

D'Ortenzio, F., Antoine, D., and Marullo, S.: Satellite-driven modeling of the upper ocean mixed layer and air-sea CO2 flux in the Mediterranean Sea, Deep-Sea Research Part I: Oceanographic Research Papers, 55, 405–434, https://doi.org/10.1016/j.dsr.2007.12.008, 2008.

D'Ortenzio, F., Taillandier, V., Claustre, H., Coppola, L., Conan, P., Dumas, F., Durrieu du Madron, X., Fourrier, M., Gogou, A., Karageorgis, A., Lefevre, D., Leymarie, E., Oviedo, A., Pavlidou, A., Poteau, A., Poulain, P. M., Prieur, L., Psarra, S., Puyo-Pay, M., Ribera d'Alcalà, M., Schmechtig, C., Terrats, L., Velaoras, D., Wagener, T., and Wimart-Rousseau, C.: BGC-Argo Floats Observe Nitrate Injection and Spring Phytoplankton Increase in the Surface Layer of Levantine Sea (Eastern Mediterranean), Geophysical Research Letters, 48, 1–11, https://doi.org/10.1029/2020GL091649, 2021.

Ducklow, H. W. and Doney, S. C.: What Is the Metabolic State of the Oligotrophic Ocean? A Debate, Ann. Rev. Mar. Sci., 5(1), 525–533, doi:10.1146/annurev-marine-121211-172331, 2013.

Ediger, D. and Yilmaz, A.: Characteristics of deep chlorophyll maximum in the Northeastern Mediterranean with respect to environmental conditions, Journal of Marine Systems, 7963, 1996.

Ediger, D., Tuˇgrul, S., and Yilmaz, A.: Vertical profiles of particulate organic matter and its relationship with chlorophyll-a in the upper layer of the NE Mediterranean Sea, Journal of Marine Systems, 55, 311–326, https://doi.org/10.1016/j.jmarsys.2004.09.003, 2005.

Estournel, C., Kondrachoff, V., Marsaleix, P., and Vehil, R.: The plume of the Rhone: Numerical simulation and remote sensing, Continental Shelf Research, 17, 899–924, https://doi.org/10.1016/S0278-4343(96)00064-7, 1997.

Estournel, C., Broche, P., Marsaleix, P., Devenon, J. L., Auclair, F., and Vehil, R.: The rhone river plume in unsteady conditions: Numerical and experimental results, Estuarine, Coastal and Shelf Science, 53, 25–38, https://doi.org/10.1006/ecss.2000.0685, 2001.

Estournel, C., De Madron, X. D., Marsaleix, P., Auclair, F., Julliand, C., and Vehil, R.: Observation and modeling of the winter coastal oceanic circulation in the Gulf of Lion under wind conditions influenced by the continental orography (FETCH experiment), Journal of Geophysical Research: Oceans, 108, 1–19, https://doi.org/10.1029/2001jc000825, 2003.

Estournel, C., Zervakis, V., Marsaleix, P., Papadopoulos, A., Auclair, F., Perivoliotis, L., and Tragou, E.: Dense water formation and cascading in the Gulf of Thermaikos (North Aegean), from observations and modelling, Continental Shelf Research, 25, 2366–2386, https://doi.org/10.1016/j.csr.2005.08.014, 2005.

Estournel, C., Testor, P., Taupier-Letage, I., Bouin, M. N., Coppola, L., Durand, P., Conan, P., Bosse, A., Brilouet, P. E., Beguery, L., Belamari, S., Béranger, K., Beuvier, J., Bourras, D., Canut, G., Doerenbecher, A., de Madron, X. D., D'Ortenzio, F., Drobinski, P., Ducrocq, V., Fourrié, N., Giordani, H., Houpert, L., Labatut, L., Brossier, C. L., Nuret, M., Prieur, L., Roussot, O., Seyfried, L., and Somot, S.: HyMeX-SOP2: The field campaign dedicated to dense water formation in the northwestern Mediterranean, Oceanography, 29,196–206, https://doi.org/10.5670/oceanog.2016.94, 2016.

Estournel, C., Marsaleix, P., and Ulses, C.: A new assessment of the circulation of Atlantic and Intermediate Waters in the Eastern Mediterranean, Progress in Oceanography, 198, 102 673, https://doi.org/10.1016/j.pocean.2021.102673, 2021.

Fach, B. A., Orek, H., Yilmaz, E., Tezcan, D., Salihoglu, I., Salihoglu, B., and Latif, M. A.: Water Mass Variability and Levantine Intermediate Water Formation in the Eastern Mediterranean between 2015-2017, Journal of Geophysical Research: Oceans, 2, https://doi.org/10.1029/2020jc016472, 2021.

Fourrier, M.: Dataset used for CANYON-MED training and validation., figshare, https://doi.org/Fourrier, Marine (2020): Dataset used for CANYON-MED training and validation. figshare. Dataset. https://doi.org/10.6084/m9.figshare.12452795.v1, 2020.

Fourrier, M., Coppola, L., Claustre, H., D'Ortenzio, F., Sauzède, R., and Gattuso, J. P.: A Regional Neural Network Approach to Estimate Water-Column Nutrient Concentrations and Carbonate System Variables in the Mediterranean Sea: CANYON-MED, Frontiers in Marine Science, 7, https://doi.org/10.3389/fmars.2020.00620, 2020.

Friedlingstein, P., Jones, M. W., Sullivan, M. O., Andrew, R. M., Bakker, D. C. E., Hauck, J., Quéré, C. L., Peters, G. P., and Peters, W.:Global Carbon Budget 2021, Earth System Science Data, 14, 1917–2005, 2022.

Galí, M., Falls, M., Claustre, H., Aumont, O., and Bernardello, R.: Bridging the gaps between particulate backscattering measurements and modeled particulate organic carbon in the ocean, Biogeosciences, 19, 1245–1275, https://doi.org/10.5194/bg-19-1245-2022, 2022

Gardner, W. D., Chung, S. P., Richardson, M. J., and Walsh, I. D.: The oceanic mixed-layer pump, Deep-Sea Research Part II, 42, https://doi.org/10.1016/0967-0645(95)00037-Q, 1995.

https://doi.org/10.5194/bg-2022-216
Preprint. Discussion started: 21 November 2022

Gogou, A., Sanchez-Vidal, A., Durrieu de Madron, X., Stavrakakis, S., Calafat, A. M., Stabholz, M., Psarra, S., Canals, M., Heussner, S., Stavrakaki, I., and Papathanassiou, E.: Reprint of: Carbon flux to the deep in three open sites of the Southern European Seas (SES), Journal of Marine Systems, 135, 170–179, https://doi.org/10.1016/j.jmarsys.2014.04.012, 2014.

Grasshoff, K., Kremling, K., and Ehrhardt, M.: Methods of seawater analysis, Marine Chemistry, 7, 86–87, https://doi.org/10.1016/0304-4203(78)90045-2, 1999.

Grignon, L., Smeed, D. A., Bryden, H. L., and Schroeder, K.: Importance of the variability of hydrographic preconditioning for deep convection in the Gulf of Lion, NW Mediterranean, Ocean Science, 6, 573–586, https://doi.org/10.5194/os-6-573-2010, 2010.

Guerzoni, S., Chester, R., Dulac, F., Herut, B., Loÿe-Pilot, M. D., Measures, C., Migon, C., Molinaroli, E., Moulin, C., Rossini, P., Saydam, C., Soudine, A., and Ziveri, P.: The role of atmospheric deposition in the biogeochemistry of the Mediterranean Sea, Progress in Oceanography, 44, 147–190, https://doi.org/10.1016/S0079-6611(99)00024-5, 1999.

Guyennon, A., Baklouti, M., Diaz, F., Palmieri, J., Beuvier, J., Lebaupin-Brossier, C., Arsouze, T., Beranger, K., Dutay, J. C., and Moutin, T.: New insights into the organic carbon export in the Mediterranean Sea from 3-D modeling, Biogeosciences, 12, 7025–7046,https://doi.org/10.5194/bg-12-7025-2015, 2015.

Hassoun, A. E. R., Fakhri, M., Raad, N., Abboud-Abi Saab, M., Gemayel, E., and De Carlo, E. H.: The carbonate system of the Eastern-most Mediterranean Sea, Levantine Sub-basin: Variations and drivers, Deep-Sea Research Part II: Topical Studies in Oceanography, 164, 54–73,https://doi.org/10.1016/j.dsr2.2019.03.008, 2019.

Hecht, A., Robinson, A. R., and Pinardi, N.: Currents, water masses, eddies and jets in the Mediterranean Levantine Basin., 1988.

Hermann, M., Somot, S., Sevault, F., Estournel, C., and Déqué, M.: Modeling the deep convection in the northwestern Mediterranean sea using an eddy-permitting and an eddy-resolving model: Case study of winter 1986-1987, Journal of Geophysical Research: Oceans, 113,1–25, https://doi.org/10.1029/2006JC003991, 2008.

Herrmann, M., Diaz, F., Estournel, C., Marsaleix, P., and Ulses, C.: Impact of atmospheric and oceanic interannual variability on the North-western Mediterranean Sea pelagic planktonic ecosystem and associated carbon cycle, Journal of Geophysical Research: Oceans, 118,5792–5813, https://doi.org/10.1002/jgrc.20405, 2013.

Herut, B. and Krom, M.: Atmospheric Input of Nutrients and Dust to the SE Mediterranean, in: Guerzoni, S., Chester, R. (eds) The Impact of Desert Dust Across the Mediterranean., pp. 349–358, springe,dordrecht, https://doi.org/10.1007/978-94-017-3354-0_35, 1996.

Hood, E. M. and Merlivat, L.: Annual to interannual variations of fCO2 in the northwestern Mediterranean Sea: Results from hourly measurements made by CARIOCA buoys, 1995-1997, Journal of Marine Research, 59, 113–131, https://doi.org/10.1357/002224001321237399, 2001.

Horton, C., Clifford, M., and Schmitz, J.: A real-time oceanographic nowcast / forecast system for the Mediterranean Sea. Journal of Geophysical Research: Oceans, 102, C11, https://doi.org/10.1029/97JC005331997.

Houpert, L., Testor, P., de Madron, X. D., Somot, S., D'Ortenzio, F., Estournel, C., and Lavigne, H.: Seasonal cycle of the mixed layer, the seasonal thermocline and the upper-ocean heat storage rate in the Mediterranean

Sea derived from observations, Progress in Oceanography, 132, 333–352, https://doi.org/10.1016/j.pocean.2014.11.004, 2015.

Kalaroni, S., Tsiaras, K., Petihakis, G., Economou-Amilli, A., and Triantafyllou, G.: Modelling the mediterranean pelagic ecosystem using the POSEIDON ecological model. Part II: Biological dynamics, Deep-Sea Research Part II: Topical Studies in Oceanography, 171, 104 711, https://doi.org/10.1016/j.dsr2.2019.104711, 2020.

Kanakidou, M., Duce, R. A., Prospero, J. M., Baker, A. R., Benitez-Nelson, C., Dentener, F. J., Hunter, K. A., Liss, P. S., Mahowald, N.,Okin, G. S., Sarin, M., Tsigaridis, K., Uematsu, M., Zamora, L. M., and Zhu, T.: Atmospheric fluxes of organic N and P to the global ocean, Global Biogeochemical Cycles, 26, 1–12, https://doi.org/10.1029/2011GB004277, 2012.

Kessouri, F., Mer, D., and Processus, M.: Cycles biogéochimiques de la Mer Méditerranée : Processus et bilans, Ph.D. thesis, Paul Sabatier,2016.

Kessouri, F., Ulses, C., Estournel, C., Marsaleix, P., Severin, T., Pujo-Pay, M., Caparros, J., Raimbault, P., Pasqueron de Fommervault, O., D'Ortenzio, F., Taillandier, V., Testor, P., and Conan, P.: Nitrogen and Phosphorus Budgets in the Northwestern Mediterranean Deep Convection Region, Journal of Geophysical Research: Oceans, 122, 9429–9454, https://doi.org/10.1002/2016JC012665, 2017.

Kessouri, F., Ulses, C., Estournel, C., Marsaleix, P., D'Ortenzio, F., Severin, T., Taillandier, V., and Conan, P.: Vertical Mixing Effects on Phytoplankton Dynamics and Organic Carbon Export in the Western Mediterranean Sea, Journal of Geophysical Research: Oceans, 123, 1647–1669, https://doi.org/10.1002/2016JC012669, 2018.

Key, R. M., Kozyr, A., Sabine, C. L., Lee, K., Wanninkhof, R., Bullister, J. L., Feely, R. A., Millero, F. J., Mordy, C., and Peng, T. H.:A global ocean carbon climatology: Results from Global Data Analysis Project (GLODAP), Global Biogeochemical Cycles, 18, 1–23, https://doi.org/10.1029/2004GB002247, 2004.

Körtzinger, A., Schimanski, J., Send, U., and Wallace, D.: The ocean takes a deep breath, Science, 306, 1337, https://doi.org/10.1126/science.1102557, 2004.

Kotta, D. and Kitsiou, D.: Chlorophyll in the eastern mediterranean sea: Correlations with environmental factors and trends, Environments MDPI, 6, https://doi.org/10.3390/environments6080098, 2019.

Kress, N., Gertman, I., and Herut, B.: Temporal evolution of physical and chemical characteristics of the water column in the Easternmost Levantine basin (Eastern Mediterranean Sea) from 2002 to 2010, Journal of Marine Systems, 135, 6–13, https://doi.org/10.1016/j.jmarsys.2013.11.016, 2014.

Krom, Brenner, S., Kress, N., Neori, A., and Gordon, L. I.: Nutrient dynamics and new production in a warm core eddy from the eastern Mediterranean Sea, Deep-Sea Research Part I, 39, 467–480, 1991.

Krom, M. D., Woodward, E. M., Herut, B., Kress, N., Carbo, P., Mantoura, R. F., Spyres, G., Thingsted, T. F., Wassmann, P., Wexels-Riser, C., Kitidis, V., Law, C., and Zodiatis, G.: Nutrient cycling in the south east Levantine basin of the eastern Mediterranean: Results from a phosphorus starved system, Deep-Sea Research Part II: Topical Studies in Oceanography, 52, 2879–2896, https://doi.org/10.1016/j.dsr2.2005.08.009, 2005.

Kubin, E., Poulain, P. M., Mauri, E., Menna, M., and Notarstefano, G.: Levantine intermediate and levantine deep water formation: An Argo float study from 2001 to 2017, Water (Switzerland), 11, https://doi.org/10.3390/w11091781, 2019.

Lacour, T., Morin, P. I., Sciandra, T., Donaher, N., Campbell, D. A., Ferland, J., and Babin, M.: Decoupling light harvesting, electron transport and carbon fixation during prolonged darkness supports rapid recovery upon re-illumination in the Arctic diatom Chaetoceros neogracilis, Polar Biology, 42, 1787–1799, https://doi.org/10.1007/s00300-019-02507-2, 2019.

Lascaratos, A., Williams, R. G., and Tragou, E.: A mixed-layer study of the formation of Levantine Intermediate Water, Journal of Geophysical Research, 98, 1993.

Lascaratos, A., Roether, W., Nittis, K., and Klein, B.: Recent changes in deep water formation and spreading in the Eastern Mediterranean Sea: A review, Progress in Oceanography, 44, 5–36, https://doi.org/10.1016/S0079-6611(99)00019-1, 1999.

Lavigne, H., D'Ortenzio, F., Migon, C., Claustre, H., Testor, P., D'Alcalà, M. R., Lavezza, R., Houpert, L., and Prieur, L.: Enhancing the comprehension of mixed layer depth control on the Mediterranean phytoplankton phenology, Journal of Geophysical Research: Oceans, 118, 3416–3430, https://doi.org/10.1002/jgrc.20251, 2013.

Lazzari, P., Solidoro, C., Ibello, V., Salon, S., Teruzzi, A., Béranger, K., Colella, S., and Crise, A.: Seasonal and inter-annual variability of plankton chlorophyll and primary production in the Mediterranean Sea: A modelling approach, Biogeosciences, 9, 217–233, https://doi.org/10.5194/bg-9-217-2012, 2012.

Ludwig, W., Bouwman, A. F., Dumont, E., and Lespinas, F.: Water and nutrient fluxes from major Mediterranean and Black Sea rivers: Past and future trends and their implications for the basin-scale budgets, Global Biogeochemical Cycles, 24, 1–14,https://doi.org/10.1029/2009GB003594, 2010.

Macías, D., Stips, A., and Garcia-Gorriz, E.: The relevance of deep chlorophyll maximum in the open Mediterranean Sea evaluated through 3D hydrodynamic-biogeochemical coupled simulations, Ecological Modelling, 281, 26–37,830 https://doi.org/10.1016/j.ecolmodel.2014.03.002, 2014.

Malanotte-Rizzoli, P., Manca, B. B., Marullo, S., D'Alcala, R., Roether, W., Theocharis, A., Bergamasco, A., Budillon, G., Sansone, E.,Civitarese, G., Conversano, F., Gertman, I., Herut, B., Kress, N., Kioroglou, S., Kontoyannis, H., Nittis, K., Klein, B., Lascaratos, A., Latif, M. A., Ozsoy, E., Robinson, A. R., Santoleri, R., Viezzoli, D., and Kovacevic, V.: The Levantine Intermediate Water Experiment (LIWEX) Group: Levantine basin - A laboratory for multiple water mass formation processes, Journal of Geophysical Research C: Oceans,108, https://doi.org/10.1029/2002jc001643, 2003.

Malanotte-Rizzoli, P., Artale, V., Borzelli-Eusebi, G. L., Brenner, S., Crise, A., Gacic, M., Kress, N., Marullo, S., Ribera D'Alcalà, M., Sofianos, S., Tanhua, T., Theocharis, A., Alvarez, M., Ashkenazy, Y., Bergamasco, A., Cardin, V., Carniel, S., Civitarese, G., D'Ortenzio, F., Font, J., Garcia-Ladona, E., Garcia-Lafuente, J. M., Gogou, A., Gregoire, M., Hainbucher, D., Kontoyannis, H., Kovacevic, V., Kraskapoulou, E., Kroskos, G., Incarbona, A., Mazzocchi, M. G., Orlic, M., Ozsoy, E., Pascual, A., Poulain, P. M., Roether, W., Rubino, A., Schroeder, K., Siokou-Frangou, J., Souvermezoglou, E., Sprovieri, M., Tintoré, J., and Triantafyllou, G.: Physical forcing and physical/biochemical variability of the Mediterranean Sea: A review of unresolved issues and directions for future research, Ocean Science, 10, 281–322, https://doi.org/10.5194/os-10-281-2014, 2014.

Manca, B., Burca, M., Giorgetti, A., Coatanoan, C., Garcia, M. J., and Iona, A.: Physical and biochemical averaged vertical profiles in the Mediterranean regions: An important tool to trace the climatology of water masses and to validate incoming data from operational oceanography, Journal of Marine Systems, 48, 83–116, https://doi.org/10.1016/j.jmarsys.2003.11.025, 2004.

https://doi.org/10.5194/bg-2022-216
Preprint. Discussion started: 21 November 2022

Many, G., Ulses, C., Estournel, C., and Marsaleix, P.: Particulate organic carbon budget of the Gulf of Lion shelf (NW Mediterranean) using a coupled hydrodynamic-biogeochemical model, Biogeosciences Discussions, pp. 1–41, https://doi.org/10.5194/bg-2021-82, 2021.

Margirier, F., Testor, P., Heslop, E., Mallil, K., Bosse, A., Houpert, L., Mortier, L., Bouin, M. N., Coppola, L., D'Ortenzio, F., Durrieu de Madron, X., Mourre, B., Prieur, L., Raimbault, P., Taillandier, V., de Madron, X., Mourre, B., Prieur, L., Raimbault, P., and Taillandier, V.: Abrupt warming and salinification of intermediate waters interplays with decline of deep convection in the Northwestern Mediterranean Sea, Scientific Reports, 10, 1–11, https://doi.org/10.1038/s41598-020-77859-5, 2020.

Marsaleix, P., Estournel, C., Kondrachoff, V., and Vehil, R.: A numerical study of the formation of the Rhone River plume, Journal of Marine Systems, 14, 99–115, https://doi.org/10.1016/S0924-7963(97)00011-0, 1998.

Marsaleix, P., Auclair, F., and Estournel, C.: Considerations on open boundary conditions for regional and coastal ocean models, Journal of Atmospheric and Oceanic Technology, 23, 1604–1613, https://doi.org/10.1175/JTECH1930.1, 2006.

Marsaleix, P., Auclair, F., Floor, J. W., Herrmann, M. J., Estournel, C., Pairaud, I., and Ulses, C.: Energy conservation issues in sigma coordinate free-surface ocean models, Ocean Modelling, 20, 61–89, https://doi.org/10.1016/j.ocemod.2007.07.005, 2008.

Martínez-Pérez, A. M., Osterholz, H., Nieto-Cid, M., Álvarez, M., Dittmar, T., and Álvarez-Salgado, X. A.: Molecular composition of dissolved organic matter in the Mediterranean Sea, Limnology and Oceanography, 62, 2699–2712, https://doi.org/10.1002/lno.10600,2017.

Marullo, S., Napolitano, E., Santoleri, R., Manca, B., and Evans, R.: Variability of Rhodes and Ierapetra Gyres during Levantine Intermediate Water Experiment: Observations and model results, Journal of Geophysical Research: Oceans, 108, 1–18,https://doi.org/10.1029/2002jc001393, 2003.

Mayot, N., D'Ortenzio, F., D'Alcalà, M. R., Lavigne, H., and Claustre, H.: Interannual variability of the Mediterranean trophic regimes from ocean color satellites, Biogeosciences, 13, 1901–1917, https://doi.org/10.5194/bg-13-1901-2016, 2016.

Mayot, N., D'Ortenzio, F., Taillandier, V., Prieur, L., de Fommervault, O. P., Claustre, H., Bosse, A., Testor, P., and Conan, P.: Physical and Biogeochemical Controls of the Phytoplankton Blooms in North Western Mediterranean Sea: A Multiplatform Approach Over a Complete Annual Cycle (2012–2013 DEWEX Experiment), Journal of Geophysical Research: Oceans, 122, 9999–10 019,https://doi.org/10.1002/2016JC012052, 2017.

Mémery, L., Lévy, M., Vérant, S., and Merlivat, L.: The relevant time scales in estimating the air-sea CO2 exchange in a mid-latitude region, Deep-Sea Research Part II: Topical Studies in Oceanography, 49, 2067–2092, https://doi.org/10.1016/S0967-0645(02)00028-0, 2002.

Menna, M. and Poulain, P. M.: Mediterranean intermediate circulation estimated from Argo data in 2003-2010, Ocean Science, 6, 331–343, https://doi.org/10.5194/os-6-331-2010, 2010.

Menna, M., Gerin, R., Notarstefano, G., Mauri, E., Bussani, A., Pacciaroni, M., and Poulain, P. M.: On the Circulation and Thermohaline Properties of the Eastern Mediterranean Sea, Frontiers in Marine Science, 8, 1–19, https://doi.org/10.3389/fmars.2021.671469, 2021.

https://doi.org/10.5194/bg-2022-216
Preprint. Discussion started: 21 November 2022

Merlivat, L., Boutin, J., Antoine, D., Beaumont, L., Golbol, M., and Vellucci, V.: Increase of dissolved inorganic carbon and decrease in pH in near-surface waters in the Mediterranean Sea during the past two decades, Biogeosciences, 15, 5653–5662, https://doi.org/10.5194/bg-15-5653-2018, 2018.

Mignot, A., Claustre, H., Uitz, J., Poteau, A., Ortenzio, F. D., and Xing, X.: Understanding the seasonal dynamics and the deep chlorophyll maximum in oligotrophic, AGU. Global Biogeochemical Cycles, 856–876, https://doi.org/10.1002/2013GB004781, 2014.

Mikolajczak, G., Estournel, C., Ulses, C., Marsaleix, P., Bourrin, F., Martín, J., Pairaud, I., Puig, P., Leredde, Y., Many, G., Seyfried, L., and Durrieu de Madron, X.: Impact of storms on residence times and export of coastal waters during a mild autumn/winter period in the Gulf of Lion, Continental Shelf Research, 207, https://doi.org/10.1016/j.csr.2020.104192, 2020.

Millot, C. and Taupier-Letage, I.: Circulation in the Mediterranean Sea, Life in the Mediterranean Sea: A Look at Habitat Changes, 5, 99–125, https://doi.org/10.1007/b107143, 2005.

Moutin, T. and Raimbault, P.: Primary production, carbon export and nutrients availability in western and eastern Mediterranean Sea in early summer 1996 (MINOS cruise), Journal of Marine Systems, 33-34, 273–288, https://doi.org/10.1016/S0924-7963(02)00062-3, 2002.

Nabat, P., Somot, S., Mallet, M., Michou, M., Sevault, F., Driouech, F., Meloni, D., Di Sarra, A., Di Biagio, C., Formenti, P., Sicard, M., Léon, J. F., and Bouin, M. N.: Dust aerosol radiative effects during summer 2012 simulated with a coupled regional aerosol-atmosphere-ocean model over the Mediterranean, Atmospheric Chemistry and Physics, 15, 3303–3326, https://doi.org/10.5194/acp-15-3303-2015, 2015.

Napolitano, E., Oguz, T., Malanotte-Rizzoli, P., Yilmaz, A., and Sansone, E.: Simulations of biological production in the Rhodes and Ionian basins of the eastern Mediterranean, Journal of Marine Systems, 24, 277–298, https://doi.org/10.1016/S0924-7963(99)00090-1, 2000.

Niewiadomska, K., Claustre, H., Prieur, L., and D'Ortenzio, F.: Submesoscale physical-biogeochemical coupling across the Ligurian Current (northwestern Mediterranean) using a bio-optical glider, Limnology and Oceanography, 53, 2210–2225,https://doi.org/10.4319/lo.2008.53.5_part_2.2210, 2008.

Nixon, S. W.: Replacing the Nile: Are anthropogenic nutrients providing the fertility once brought to the Mediterranean by a great river?,Ambio, 32, 30–39, https://doi.org/10.1579/0044-7447-32.1.30, 2003.

Omand, M. M., Asaro, E. A. D., Lee, C. M., Perry, M. J., Briggs, N., Cetini, I., and Mahadevan, A.: Eddy-driven subduction exports particulate organic carbon from the spring bloom, Science, 348, 2015.

Oschlies, A.: Feedbacks of biotically induced radiative heating on upper-ocean heat budget, circulation, and biological production in a coupled ecosystem-circulation model, Journal of Geophysical Research: Oceans, 109, 1–12, https://doi.org/10.1029/2004JC002430, 2004.

Ozer, T., Gertman, I., Kress, N., Silverman, J., and Herut, B.: Interannual thermohaline (1979–2014) and nutrient (2002–2014) dynamics in the Levantine surface and intermediate water masses, SE Mediterranean Sea, Global and Planetary Change, 151, 60–67, https://doi.org/10.1016/j.gloplacha.2016.04.001, 2016.

Ozer, T., Rahav, E., Gertman, I., Sisma-Ventura, G., Silverman, J., and Herut, B.: Relationship between thermohaline and biochemical patterns in the levantine upper and intermediate water masses, Southeastern Mediterranean Sea (2013–2021), Frontiers in Marine Science, 9, 1–11, https://doi.org/10.3389/fmars.2022.958924, 2022.

https://doi.org/10.5194/bg-2022-216
Preprint. Discussion started: 21 November 2022

Özsoy, E., Hecht, A., and Ünlüata, : Circulation and hydrography of the Levantine Basin. Results of POEM coordinated experiments 1985-1986, Progress in Oceanography, 22, 125–170, https://doi.org/10.1016/0079-6611(89)90004-9, 1989.

Özsoy, E., Hecht, A., Ünlüata, , Brenner, S., Oˇguz, T., Bishop, J., Latif, M. A., and Rozentraub, Z.: A review of the Levantine Basin circulation and its variability during 1985-1988, Dynamics of Atmospheres and Oceans, 15, 421–456, https://doi.org/10.1016/0377-0265(91)90027-D, 1991.

Özsoy, E., Hecht, A., Ünlüata, , Brenner, S., Sur, H. I., Bishop, J., Latif, M. A., Rozentraub, Z., and Oˇguz, T.: A synthesis of the Levantine Basin circulation and hydrography, 1985-1990, Deep-Sea Research Part II, 40, 1075–1119, https://doi.org/10.1016/0967-0645(93)90063-S, 1993.

Palevsky, H. I. and Nicholson, D. P.: The North Atlantic Biological Pump Insights from the ocean observatoriess initiative irminger sea array, Oceanography, 31, 42–49, 2018.

Palevsky, H. I. and Quay, P. D.: Influence of biological carbon export on ocean carbon uptake over the annual cycle across the North Pacific Ocean, Global Biogeochemical Cycles, 31, 81–95, https://doi.org/10.1002/2016GB005527, 2017.

Palmiéri, J., Dutay, J.-C., D'Ortenzio, F., Houpert, L., and Bopp, L.: The Mediterranean subsurface chlorophyll dynamic and its impact on the Mediterranean bioregions, Progress in Oceanography, 2016.

Pasqueron De Fommervault, O., D'Ortenzio, F., Mangin, A., Serra, R., Migon, C., Claustre, H., Lavigne, H., Ribera D'Alcalà, M., Prieur, L., Taillandier, V., Schmechtig, C., Poteau, A., Leymarie, E., Dufour, A., Besson, F., and Obolensky, G.: Seasonal variability of nutrient concentrations in the Mediterranean Sea: Contribution of Bio-Argo floats, Journal of Geophysical Research: Oceans, 120, 8528–8550,https://doi.org/10.1002/2015JC011103, 2015.910

Pedrosa-Pàmies, R., Sanchez-Vidal, A., Canals, M., Lampadariou, N., Velaoras, D., Gogou, A., Parinos, C., and Calafat, A.: Enhanced carbon export to the abyssal depths driven by atmosphere dynamics, Geophysical Research Letters, 43, 8626–8636, https://doi.org/10.1002/2016GL069781, 2016.

Petihakis, G., Triantafyllou, G., Tsiaras, K., Korres, G., Pollani, A., and Hoteit, I.: Eastern Mediterranean biogeochemical flux model -Simulations of the pelagic ecosystem, Ocean Science, 5, 29–46, https://doi.org/10.5194/os-5-29-2009, 2009.

Petrenko, A., Dufau, C., and Estournel, C.: Barotropic eastward currents in the western Gulf of Lion, north-western Mediterranean Sea, during stratified conditions, Journal of Marine Systems, 74, 406–428, https://doi.org/10.1016/j.jmarsys.2008.03.004, 2008.

Poulos, S. E., Drakopoulos, P. G., and Collins, M. B.: Seasonal variability in sea surface oceanographic conditions in the Aegean Sea (Eastern Mediterranean), Journal of Marine Systems, 13, 225–244, 1997.

Powley, H. R., Krom, M. D., and Van Cappellen, P.: Understanding the unique biogeochemistry of the Mediterranean Sea: Insights from a coupled phosphorus and nitrogen model, Global Biogeochemical Cycles, 31, 1010–1031, https://doi.org/10.1002/2017GB005648, 2017.

Pujo-Pay, M., Conan, P., Oriol, L., Cornet-Barthaux, V., Falco, C., Ghiglione, J. F., Goyet, C., Moutin, T., and Prieur, L.: Integrated survey of elemental stoichiometry (C, N, P) from the western to eastern Mediterranean Sea, Biogeosciences, 8, 883–899, https://doi.org/10.5194/bg-8-883-2011, 2011.

Reale, M., Cossarini, G., Lazzari, P., Lovato, T., Bolzon, G., Masina, S., Solidoro, C., and Salon, S.: Acidification, deoxygenation, and nutrient and biomass declines in a warming Mediterranean Sea, Biogeosciences, 19, 4035–4065, https://doi.org/10.5194/bg-19-4035-2022, 2022.

Ribera d'Alcalà, M., Civitarese, G., Conversano, F., and Lavezza, R.: Nutrient ratios and fluxes hint at overlooked processes in the Mediterranean Sea, Journal of Geophysical Research: Oceans, 108, https://doi.org/10.1029/2002jc001650, 2003.

Richon, C., Dutay, J. C., Dulac, F., Wang, R., Balkanski, Y., Nabat, P., Aumont, O., Desboeufs, K., Laurent, B., Guieu, C., Raimbault, P., and Beuvier, J.: Modeling the impacts of atmospheric deposition of nitrogen and desert dust-derived phosphorus on nutrients and biological budgets of the Mediterranean Sea, Progress in Oceanography, 163, 21–39, https://doi.org/10.1016/j.pocean.2017.04.009, 2017.

Richon, C., Dutay, J. C., Dulac, F., Wang, R., and Balkanski, Y.: Modeling the biogeochemical impact of atmospheric phosphate deposition from desert dust and combustion sources to the Mediterranean Sea, Biogeosciences, 15, 2499–2524, https://doi.org/10.5194/bg-15-2499-2018, 2018.

Ridame, C. and Guieu, C.: Saharan input of phosphate to the oligotrophic water of the open western Mediterranean sea, Limnology and Oceanography, 47, 856–869, https://doi.org/10.4319/lo.2002.47.3.0856, 2002.

Robinson, A., Leslie, W., Theocharis, A., and Lascaratos, A.: Mediterranean Sea Circulation, Encyclopedia of Ocean Sciences, pp. 1689–1705, https://doi.org/10.1006/rwos.2001.0376, 2001.

Robson, B. J.: State of the art in modelling of phosphorus in aquatic systems: Review, criticisms and commentary, Environmental Modelling and Software, 61, 339–359, https://doi.org/10.1016/j.envsoft.2014.01.012, 2014.

Salgado-Hernanz, P. M., Racault, M. F., Font-Muñoz, J. S., and Basterretxea, G.: Trends in phytoplankton phenology in the Mediterranean Sea based on ocean-colour remote sensing, Remote Sensing of Environment, 221, 50–64, https://doi.org/10.1016/j.rse.2018.10.036, 2019.

Sanders, R., Henson, S. A., Koski, M., De La Rocha, C. L., Painter, S. C., Poulton, A. J., Riley, J., Salihoglu, B., Visser, A., Yool, A., Bellerby, R., and Martin, A. P.: The Biological Carbon Pump in the North Atlantic, Progress in Oceanography, 129, 200–218, https://doi.org/10.1016/j.pocean.2014.05.005, 2014.

Santinelli: DOC in the Mediterranean Sea, Biogeochemistry of Marine Dissolved Organic Matter: Second Edition, pp. 579–608, https://doi.org/10.1016/B978-0-12-405940-5.00013-3, 2015.

Santinelli, Nannicini, L., and Seritti, A.: DOC dynamics in the meso and bathypelagic layers of the Mediterranean Sea, Deep-Sea Research Part II: Topical Studies in Oceanography, 57, 1446–1459, https://doi.org/10.1016/j.dsr2.2010.02.014, 2010.

Santinelli, C., Hansell, D. A., and Ribera d'Alcalà, M.: Influence of stratification on marine dissolved organic carbon (DOC) dynamics: The Mediterranean Sea case, Progress in Oceanography, 119, 68–77, https://doi.org/10.1016/j.pocean.2013.06.001, 2013.

Siokou-Frangou, I., Gotsis-Skretas, O., Christou, E. D., and Pagou, K.: Plankton Characteristics in the Aegean, Ionian and NW Levantine Seas, The Eastern Mediterranean as a Laboratory Basin for the Assessment of Contrasting Ecosystems, pp. 205–223, https://doi.org/10.1007/978-94-011-4796-5_15, 1999.

https://doi.org/10.5194/bg-2022-216
Preprint. Discussion started: 21 November 2022

Siokou-Frangou, I., Christaki, U., Mazzocchi, M. G., Montresor, M., Ribera D'Alcala, M., Vaque, D., and Zingone, A.: Plankton in the open mediterranean Sea: A review, Biogeosciences, 7, 1543–1586, https://doi.org/10.5194/bg-7-1543-2010, 2010.

Soetaert, K., Middelburg, J. J., Herman, P. M., and Buis, K.: On the coupling of benthic and pelagic biogeochemical models, Earth Science Reviews, 51, 173–201, https://doi.org/10.1016/S0012-8252(00)00004-0, 2000.

Solidoro, C., Cossarini, G., Lazzari, P., Galli, G., Bolzon, G., Somot, S., and Salon, S.: Modeling Carbon Budgets and Acidification in the Mediterranean Sea Ecosystem Under Contemporary and Future Climate, Frontiers in Marine Science, 8, 1–15, https://doi.org/10.3389/fmars.2021.781522, 2022.

Somot, S., Sevault, F., Déqué, M., Somot, S., Sevault, F., and Déqué, M.: Transient climate change scenario simulation of the Mediterranean Sea for the 21st century using a high-resolution ocean circulation model To cite this version : HAL Id : hal-00195045 Transient climate change scenario simulation of the Mediterranean Sea f, Climate Dynamics, 27, 851–879, 2006.

Soto-Navarro, J., Jordá, G., Amores, A., Cabos, W., Somot, S., Sevault, F., Macías, D., Djurdjevic, V., Sannino, G., Li, L., and Sein, D.:Evolution of Mediterranean Sea water properties under climate change scenarios in the Med-CORDEX ensemble, Climate Dynamics, 54, 2135–2165, https://doi.org/10.1007/s00382-019-05105-4, 2020.

Sur, H., Ozsoy, E., and Unluata, U.: Simultaneous deep and intermediate depth convection in the Northem Levantine Sea ,, oceanologica, 16, 33–43, 1992.

Taillandier, V., D'Ortenzio, F., and Antoine, D.: Carbon fluxes in the mixed layer of the Mediterranean Sea in the 1980s and the 2000s, Deep-Sea Research Part I: Oceanographic Research Papers, 65, 73–84, https://doi.org/10.1016/j.dsr.2012.03.004, 2012.

Taillandier, V., D'Ortenzio, F., Prieur, L., Conan, P., Coppola, L., Cornec, M., Dumas, F., Durrieu de Madron, X., Fach, B., Fourrier, M., Gentil, M., Hayes, D., Husrevoglu, S., Legoff, H., Le Ster, L., Örek, H., Ozer, T., Poulain, P. M., Pujo-Pay, M., Ribera d'Alcalà, M., Salihoglu, B., Testor, P., Velaoras, D., Wagener, T., and Wimart-Rousseau, C.: Sources of the Levantine Intermediate Water in Winter 2019, Journal of Geophysical Research: Oceans, 127, 1–19, https://doi.org/10.1029/2021JC017506, 2022.

Tanhua, T., Hainbucher, D., Schroeder, K., Cardin, V., Álvarez, M., and Civitarese, G.: The Mediterranean Sea system: A review and an introduction to the special issue, Ocean Science, 9, 789–803, https://doi.org/10.5194/os-9-789-2013, 2013.

The POEM group: General circulation of the Eastern Mediterranean, Earth Science Reviews, 32, 285–309, https://doi.org/10.1016/0012-8252(92)90002-B, 1992.

Theocharis, A., Georgopoulos, D., Lascaratos, A., and Nittis, K.: Water masses and circulation in the central region of the Eastern Mediterranean, Deep-Sea Research II, 40, 1121–1142, 1993.

Thomas, L. N. and Lee, C. M.: Intensification of Ocean Fronts by Down-Front Winds, Journal of Physical Oceanography, 35, 1086–1102,2005.

Touratier, F. and Goyet, C.: Decadal evolution of anthropogenic CO2 in the northwestern Mediterranean Sea from the mid-1990s to the mid-2000s, Deep-Sea Research Part I: Oceanographic Research Papers, 56, 1708–1716, https://doi.org/10.1016/j.dsr.2009.05.015, 2009.

Tuˇgrul, S., Be ¸siktepe, T., and Salihoˇglu, I.: Nutrient exchange fluxes between the Aegean and Black Seas through the marmara sea, Mediterranean Marine Science, 3, 33–42, https://doi.org/10.12681/mms.256, 2002.

Uitz, J., Stramski, D., Gentili, B., D'Ortenzio, F., and Claustre, H.: Estimates of phytoplankton class-specific and total primary production in the Mediterranean Sea from satellite ocean color observations, Global Biogeochemical Cycles, 26, 1–10,https://doi.org/10.1029/2011GB004055, 2012.

Ulses, C., Estournel, C., Bonnin, J., Durrieu de Madron, X., and Marsalei, P.: Impact of storms and dense water cascading on shelf-slope exchanges in the Gulf of Lion (NW Mediterranean), Journal of Geophysical Research: Oceans, 113, https://doi.org/10.1029/2006JC003795,2008.

Ulses, C., Estournel, C., Kessouri, F., Hermann, M., and Marsaleix, P.: Modeling, Budget of organic carbon in the North-Western Mediterranean open sea over the period 2004–2008 using 3-D coupled physical Modeling, Journal of Geophysical Research : Oceans, 121,7026–7055, https://doi.org/10.1002/2016JC011818, 2016.

Ulses, C., Estournel, C., Fourrier, M., Coppola, L., Kessouri, F., Lefèvre, D., and Marsaleix, P.: Oxygen budget of the north-western Mediterranean deep-convection region, Biogeosciences, 18, 937–960, https://doi.org/10.5194/bg-18-937-2021, 2021.

Ulses C. et al.: Seasonal dynamics and annual budget of dissolved inorganic carbon in the north-western Mediterranean deep convection region. To be submitted to Biogeosciences Discussion.

Velaoras, D., Krokos, G., Nittis, K., & Theocharis, A.: Dense intermediate water outflow from the Cretan Sea: A salinity driven, recurrent phenomenon, connected to thermohaline circulation changes. Journal of Geophysical Research: Oceans, 119, 3868–3882. https://doi.org/10.1002/2014JC009937, 2014.

Vidussi, F., Claustre, H., Manca, B. B., Luchetta, A., and Jean-Claude, M.: Phytoplankton pigment distribution in relation to upper thermocline circulation in the eastern Mediterranean Sea during winter, Journal of Geophysical Research, 106, 939–956, 2001.

Vidussi, F., Mostajir, B., Fouilland, E., Le Floc'H, E., Nouguier, J., Roques, C., Got, P., Thibault-Botha, D., Bouvier, T., and Troussellier, M.: Effects of experimental warming and increased ultraviolet B radiation on the Mediterranean plankton food web, Limnology and Oceanography, 56, 206–218, https://doi.org/10.4319/lo.2011.56.1.0206, 2011.

Wimart-Rousseau, C., Wagener, T., Álvarez, M., Moutin, T., Fourrier, M., Coppola, L., Niclas-Chirurgien, L., Raimbault, P., D'Ortenzio, F.,Durrieu de Madron, X., Taillandier, V., Dumas, F., Conan, P., Pujo-Pay, M., and Lefèvre, D.: Seasonal and Interannual Variability of the CO2 System in the Eastern Mediterranean Sea: A Case Study in the North Western Levantine Basin, Frontiers in Marine Science, 8, 1–18, https://doi.org/10.3389/fmars.2021.649246, 2021.

Yilmaz, A. and Tugrul, S.: The effect of cold- and warm-core eddies on the distribution and stoichiometry of dissolved nutrients in the northeastern Mediterranean, Journal of Marine Systems, 16, 253–268, https://doi.org/10.1016/S0924-7963(97)00022-5, 1998.

Yilmaz, A., Ediger, D., Basturk, O., and Tugrul, S.: Phytoplankton fluorescence and deep chlorophyll maxima in the northeastern Mediterranean, Oceanologica Acta, 17, 69–77, 1994.

https://doi.org/10.5194/bg-2022-216
Preprint. Discussion started: 21 November 2022

Figures

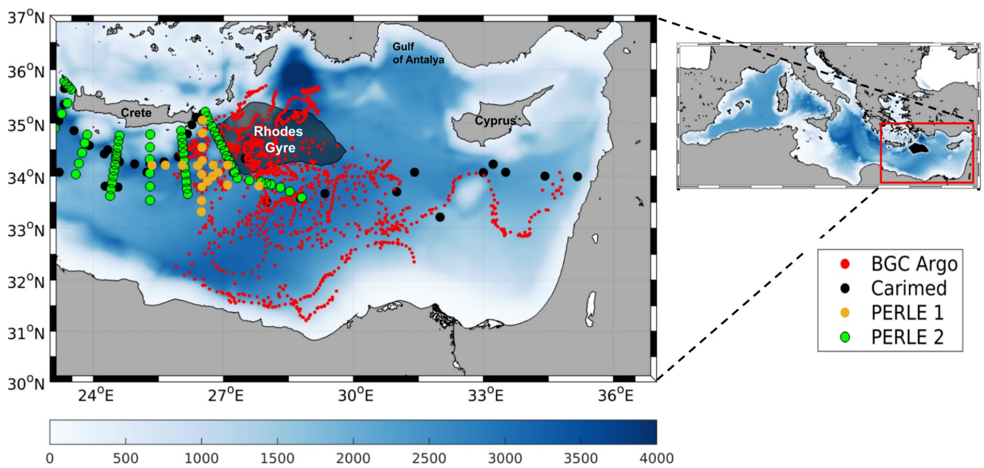

1265 **Figure 1: Model domain (right) and bathymetry (m) in the Mediterranean Sea and Levantine Basin. Red, black, yellow and green dots indicate positions of BGC-Argo floats, CARIMED, PERLE 1 and PERLE 2 cruise data, respectively, from 2013 to 2020. The black patch represents the Rhodes Gyre.**

https://doi.org/10.5194/bg-2022-216
Preprint. Discussion started: 21 November 2022

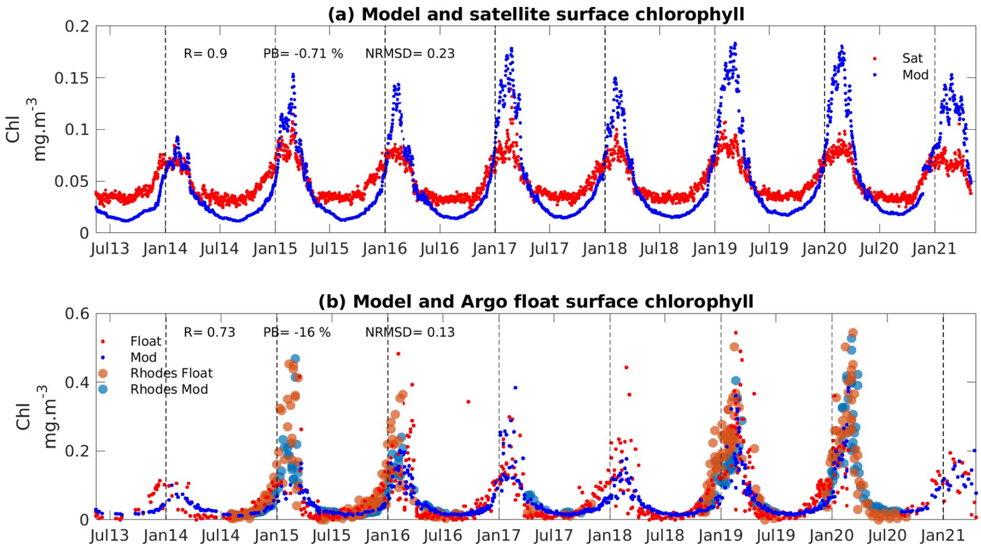

1270 **Figure 2: Time series of (a) modeled (in blue) and satellite (in red) surface chlorophyll-a concentration (mg m^{-3}) averaged over the Levantine Basin, and of (b) modeled (in blue) and BGC-Argo float (in red) surface chlorophyll-a concentration (mg m^{-3}) in the Levantine Basin; light-colored dots represent data located in the Rhodes Gyre. Coefficient correlation (R), percent bias (PB) and Normalized Root Mean Square Deviation (NRMSD) between model outputs and observations are indicated in (a) and (b).**

35

https://doi.org/10.5194/bg-2022-216
Preprint. Discussion started: 21 November 2022

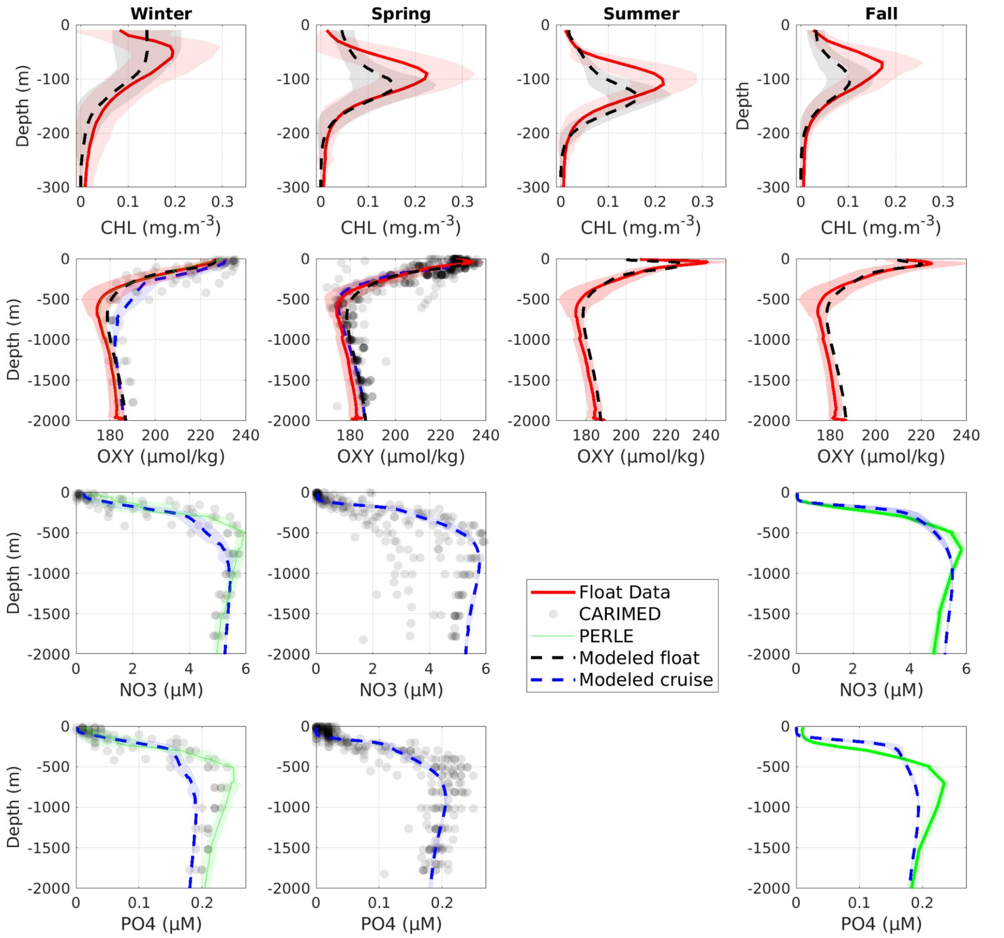

1275 **Figure 3: Comparison over the Levantine Sea between observed (gray points for CARIMED, green lines for PERLE1 and PERLE2, red line for BGC-Argo float data) and modeled (blue and black lines) profiles of chlorophyll (mg Chl m^{-3}), dissolved oxygen (µmol kg^{-1}), nitrate (µM) and phosphate (µM) concentrations, averaged by season (winter: 21 December to 20 March, spring: 21 March to 20 June, summer: 21 June to 20 September, fall: 21 September to 20 December). Shaded areas represent standard deviation.**

https://doi.org/10.5194/bg-2022-216
Preprint. Discussion started: 21 November 2022

Biogeosciences
Discussions

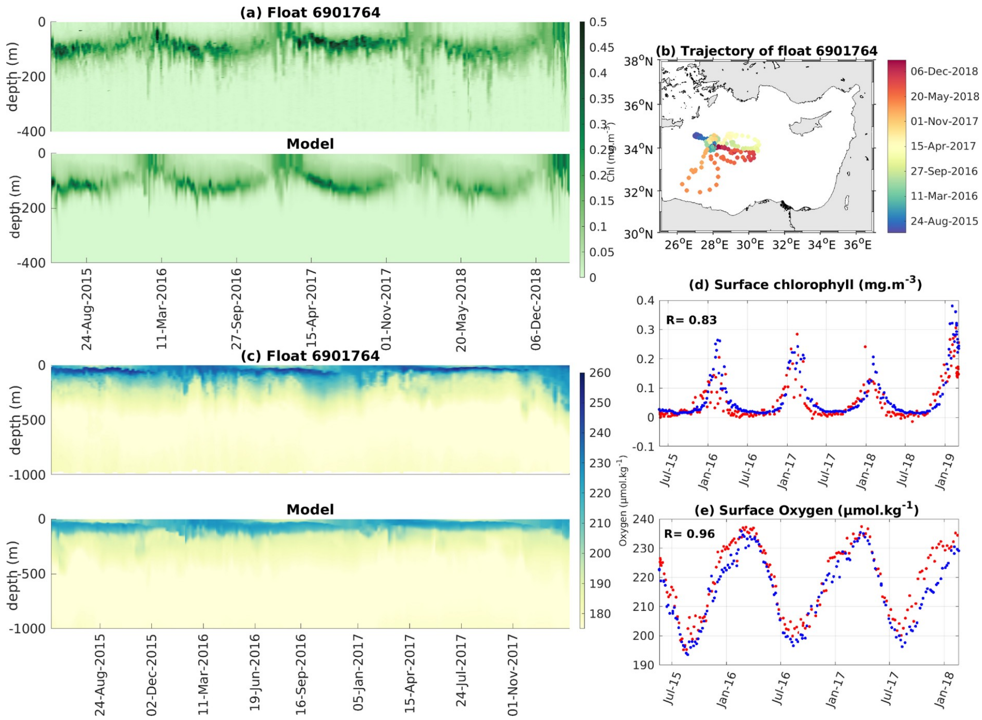

1280 **Figure 4: Time evolution of BGC-Argo float 6901764 observed and modeled data: (a) Hovmöller diagrams of chlorophyll concentration (mg m^{-3}), (b) trajectory of the BGC-Argo float, (c) Hovmöller diagrams of dissolved oxygen concentration (µmol kg^{-1}), (d) surface chlorophyll (mg m^{-3}) in the first 10 m, (e) surface dissolved oxygen (µmol kg^{-1}) observed in the first 10 m. Red dots represent the float data and the blue dots the model outputs in (d) and (e).**

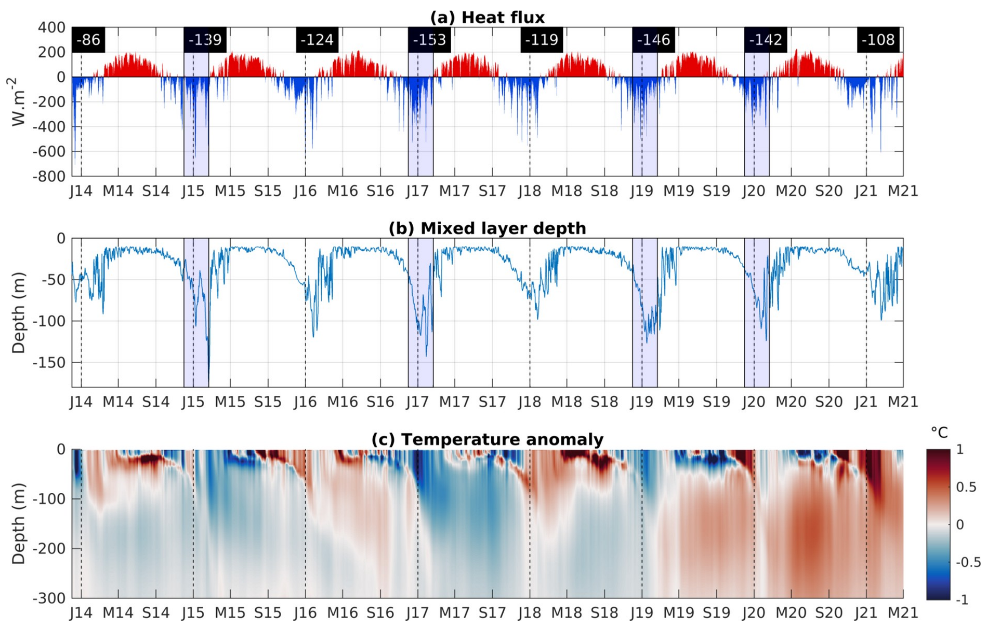

Figure 5: Time series of modeled (a) surface heat fluxes (W m^{-2}), (b) mixed layer depth (m) and (c) temperature anomaly (°C), averaged over the Rhodes Gyre area. The winter (December-January-February) mean heat loss is

https://doi.org/10.5194/bg-2022-216
Preprint. Discussion started: 21 November 2022

indicated in black rectangles in (a). J: January M: May S: September. Winters with strong heat loss and deeper mixed layers are emphasized in blue in (a) and (b).

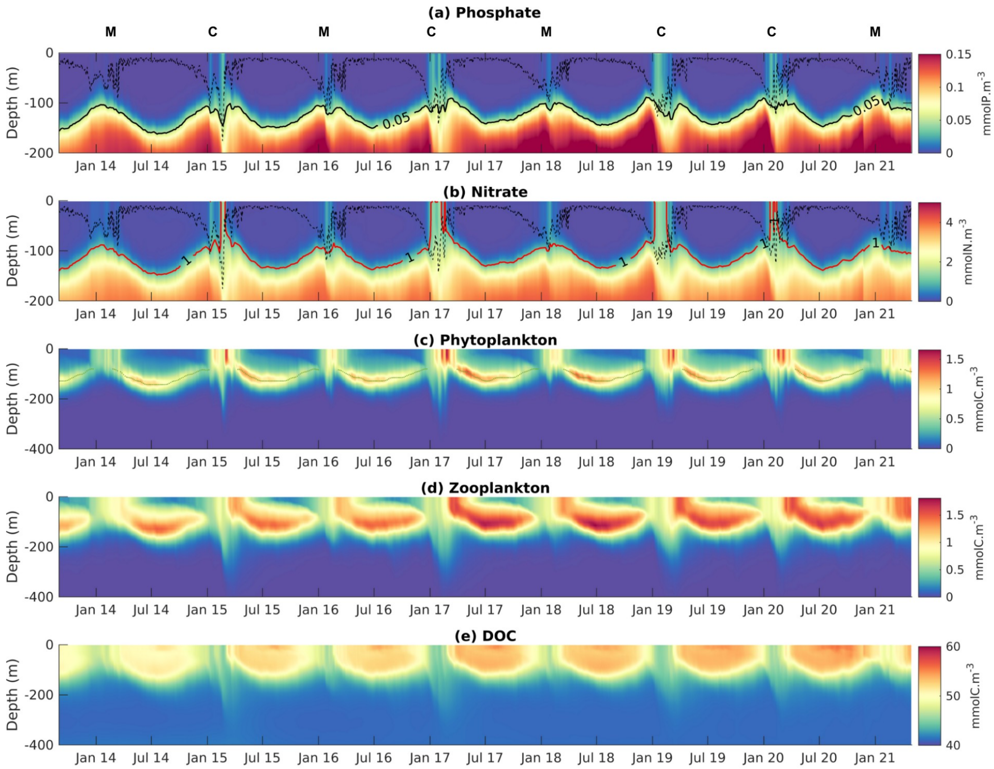

1285 **Figure 6: Hovmöller diagrams of (a) phosphate (mmol P m^{-3}), (b) nitrate (mmol N m^{-3}), (c) phytoplankton (mmol C m^{-3}), (d) zooplankton (mmol C m^{-3}) and (d) dissolved organic carbon (mmol C m^{-3}) concentrations averaged over the Rhodes Gyre, from December 2013 to 2021. The black dotted line in (a) and (b) indicates the mixed layer depth. The red line represents the depth of the nitracline in (b), and the black one of the phosphacline in (a). The green dotted line in (c) indicates the deep chlorophyll maximum. C refers to cold winter years and M to mild winter years.**

https://doi.org/10.5194/bg-2022-216
Preprint. Discussion started: 21 November 2022

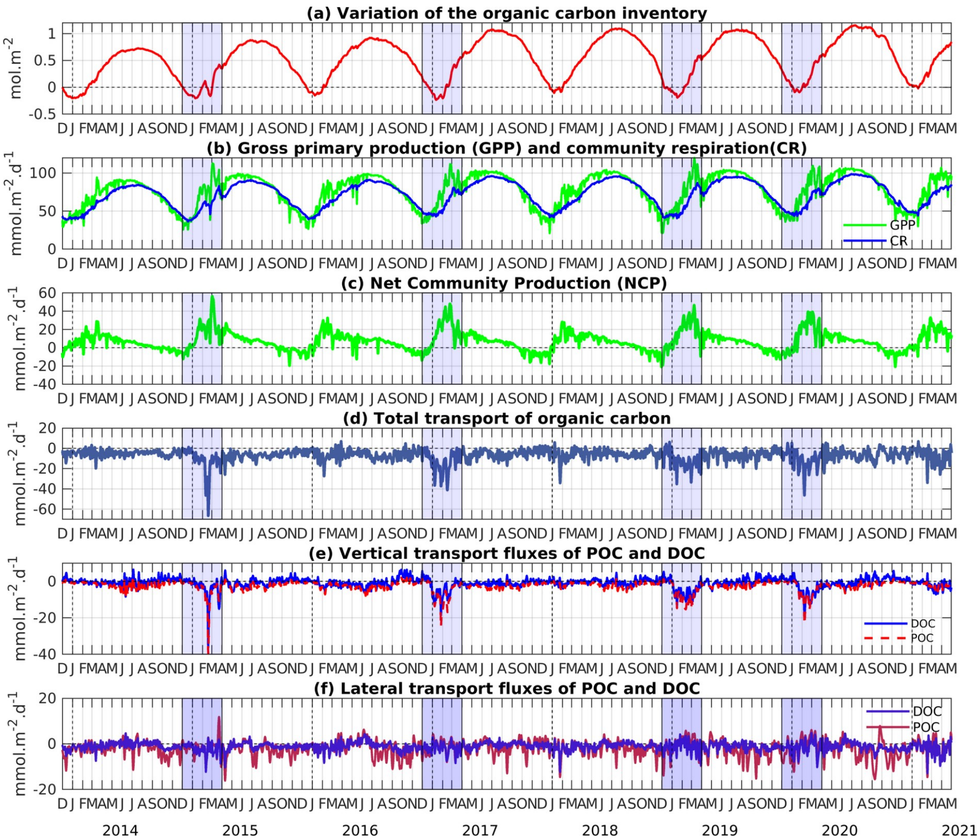

1290 **Figure 7: Time evolution of (a) the variation of the organic carbon inventory (from 1st December 2013, mol C m^{-2}), (b) gross primary production (GPP) (in green), and community respiration (CR) in the surface layer (in blue) (mmol C m^{-2} d^{-1}), (c) net community production (NCP) (mmol C m^{-2} d^{-1}), (d) total transport of organic carbon at the limits of the area (mmol C m^{-2} d^{-1}), (e) vertical transport fluxes of POC and DOC at the base of the surface layer (mmol C m^{-2} d^{-1}) and (f) lateral transport fluxes of POC and DOC at the limits of the area (mmol C m^{-2} d^{-1}), averaged over the**
1295 **Rhodes Gyre surface layer (0-150 m). Cold winters/early springs are emphasized in blue.**

https://doi.org/10.5194/bg-2022-216
Preprint. Discussion started: 21 November 2022

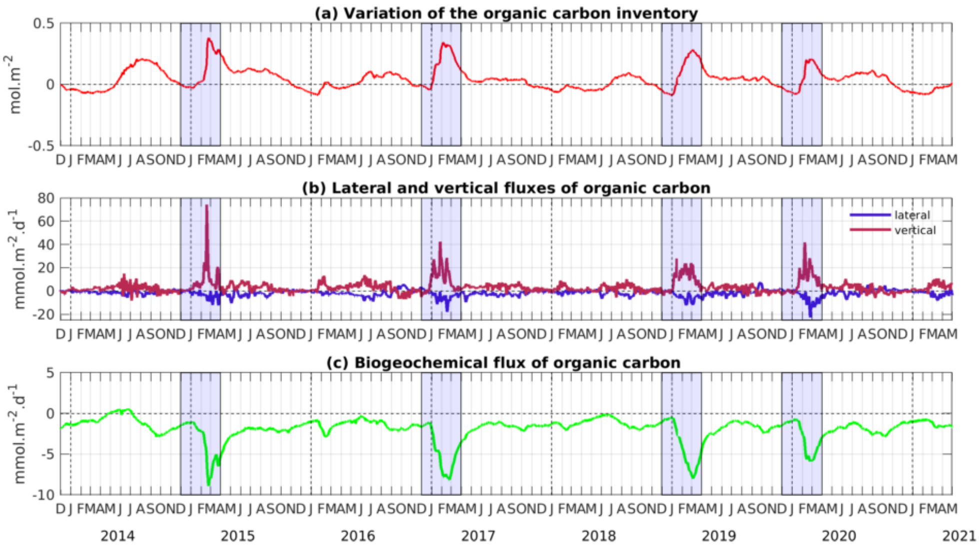

Figure 8: Time evolution of (a) variation of the organic carbon inventory (from 1st December 2013, mol C m^{-2}), (b) lateral and vertical transport fluxes of organic carbon (mmol C m^{-2} d^{-1}) at the limits of the area and (c) biogeochemical flux of organic carbon (mmol C m^{-2} d^{-1}), averaged over the Rhodes Gyre intermediate layer (150-400 m). Cold winters/early springs are emphasized in blue.

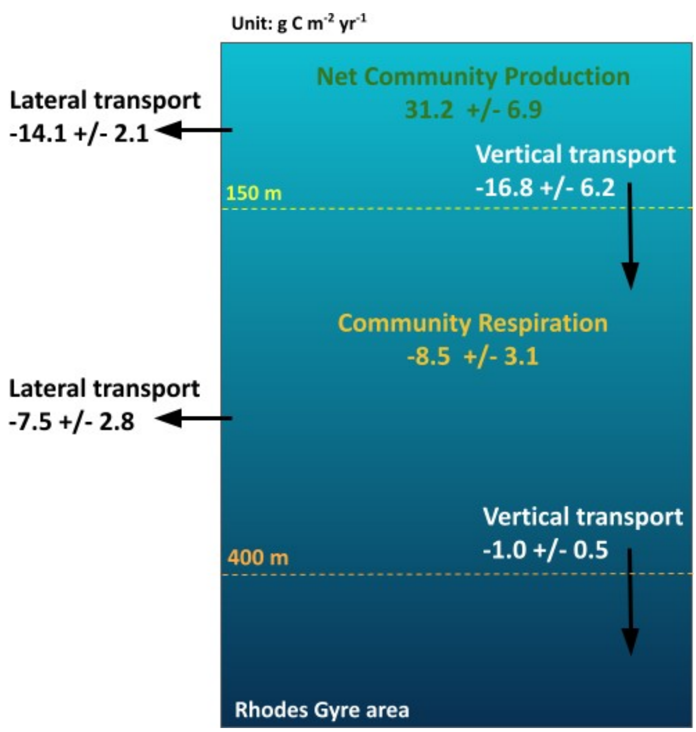

1300 **Figure 9: Annual organic carbon budget (g C m^{-2} yr^{-1}) in the surface and intermediate layers of the Rhodes Gyre for the seven year period 2013-2020.**

https://doi.org/10.5194/bg-2022-216
Preprint. Discussion started: 21 November 2022

Biogeosciences Discussions

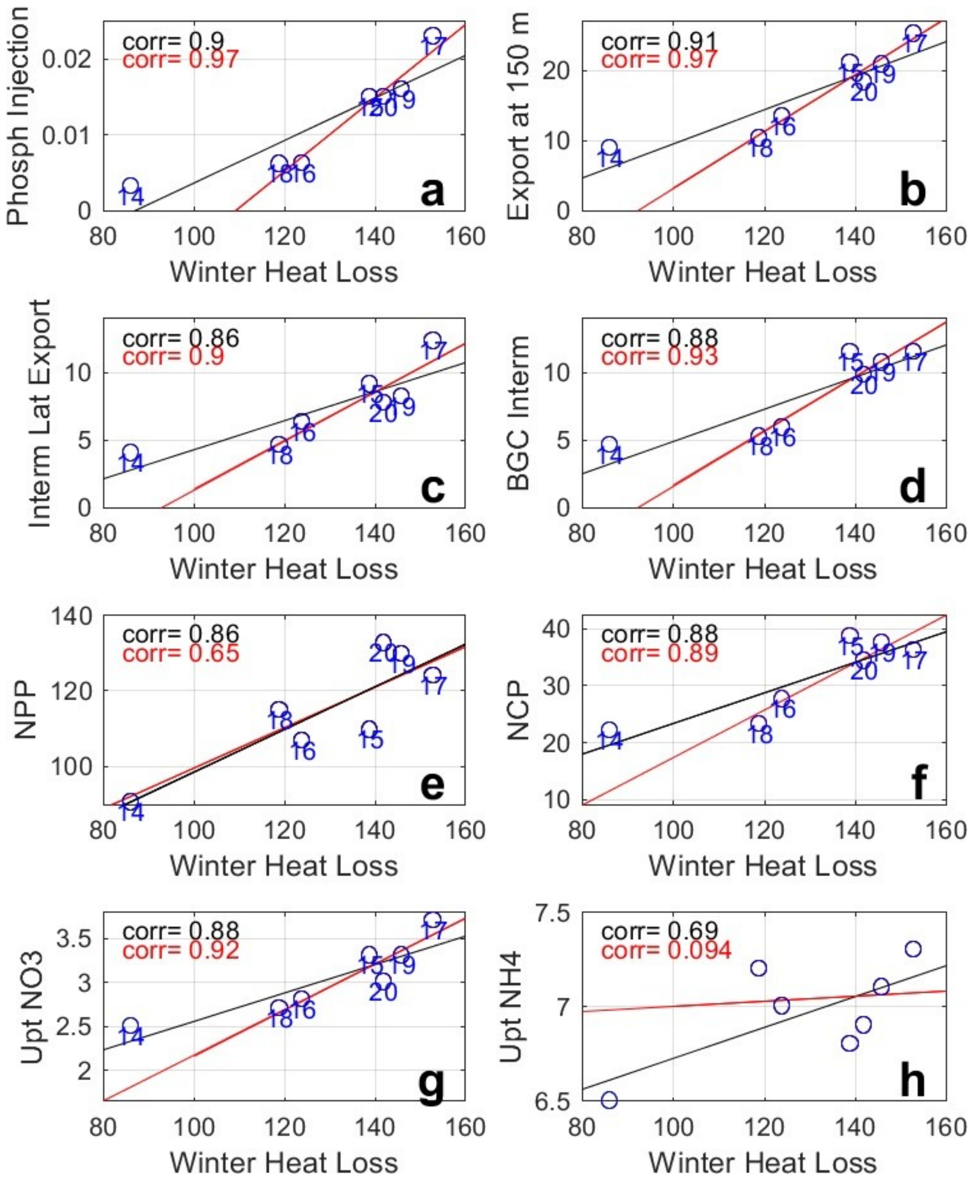

Figure 10: Scatter-plot of winter surface heat loss (W m^{-2}) vs. (a) winter phosphate injection (mol P m^{-2}) into the surface layer and mean annual values of (b) downward export of OC (Organic Carbon) at 150 m (gC m^{-2} yr^{-1}),, (c) lateral export from the intermediate layer (gC m^{-2} yr^{-1}),, (d) biogeochemical consumption in the intermediate layer (gC .m^{-2} .yr^{-1}), (e) NPP, (f) NCP (gC m^{-2} yr^{-1}), (g,h) uptake of nitrate and ammonium (mmol N m^{-2} yr^{-1}). The years are identified by the numbers in blue, e.g. 14 stands for 2013-14. The black line shows the seven years linear regression and the red line shows the linear regression when excluding 2013-14. The corresponding correlations are shown with the same color code.

https://doi.org/10.5194/bg-2022-216
Preprint. Discussion started: 21 November 2022

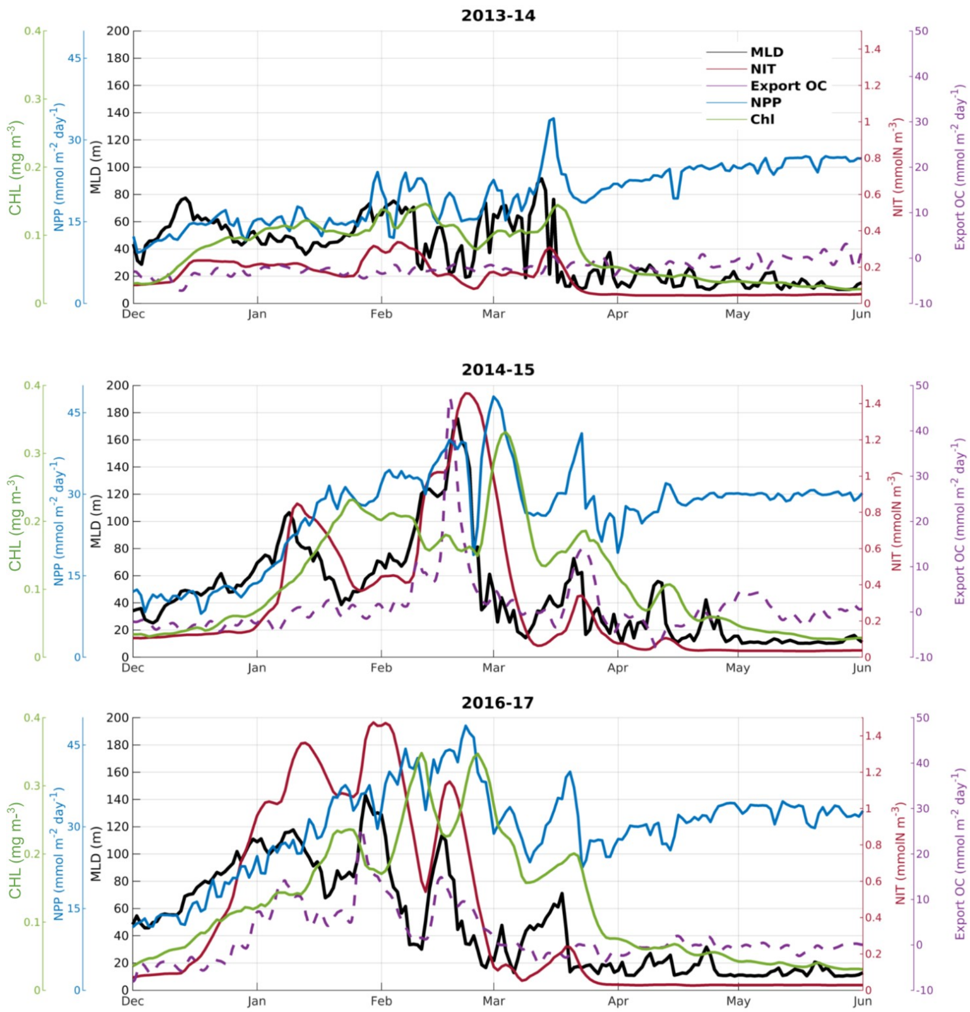

Figure 11: Annual cycle of the Mixed Layer Depth (MLD, m) (black), surface chlorophyll (CHL, mg m^{-3}) (green) and nitrate (NIT, mmol N m^{-3}) (red) concentration, net primary production (NPP, mmol C m^{-2} day^{-1}) (blue) in the upper layer (0-150 m), and the organic carbon export (mmol C m^{-2} day^{-1}) at 150 m depth (purple), for years 2013-14, 2014-15, 2016-17.

https://doi.org/10.5194/bg-2022-216
Preprint. Discussion started: 21 November 2022

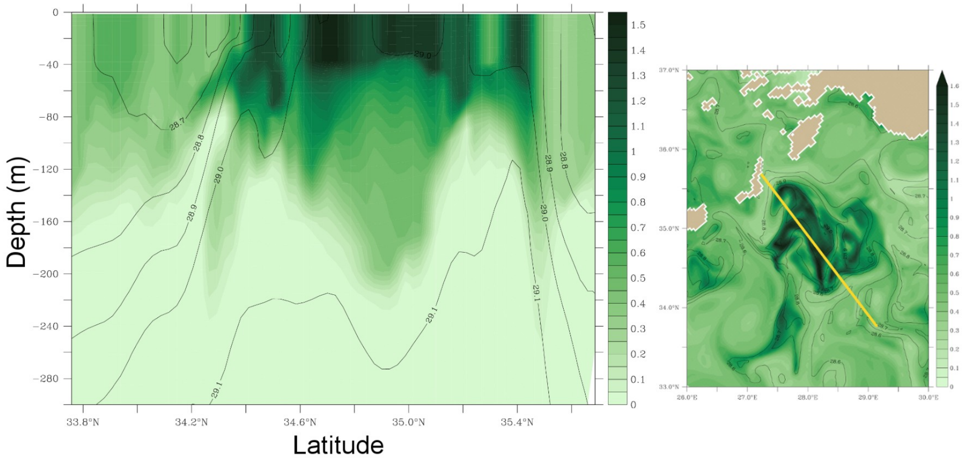

Figure 12: Vertical section of phytoplankton concentration (expressed in mmol C m^{-3}) across the Rhodes Gyre on March 27, 2015. The potential density anomaly (kg m^{-3}) is overlaid with contours. The position of the section is indicated on the map of surface phytoplankton (right panel).

https://doi.org/10.5194/bg-2022-216
Preprint. Discussion started: 21 November 2022

Tables

Table 1. Amount of nutrients injected into the surface layer in winter (December - January - February) in the Rhodes Gyre; annual biogeochemical carbon flows (gross and net primary production (GPP and NPP), net community production (NCP), community respiration (CR)), downward export flux of particulate and dissolved organic carbon (POC and DOC) at 150 and 400 m for the different years and averaged over the 7-year period, estimated from the model. Positive values correspond to an input for the considered layer of the study area. The annual budget is calculated from December.

			Units	2013-14	2014-15	2015-16	2016-17	2017-18	2018-19	2019-20	Mean (SD)
Surface layer (0 - 150m)	**Winter (DJF)**	Amount of nitrate injected in winter in the surface layer	*mol N* m^{-2}	0.09	0.33	0.14	0.47	0.14	0.31	0.30	0.25 (0.14)
		Amount of phosphate injected in winter in the surface layer	*mol P* m^{-2}	0.003	0.015	0.006	0.023	0.006	0.016	0.015	0.012 (0.007)
	Annual	GPP	$gC.m^{-2}.yr^{-1}$	298.7	330.2	328.8	350.3	337.9	354.2	357.9	336.9 (20.4)
		CR	$gC.m^{-2}.yr^{-1}$	281.5	303.8	307.9	326.3	320.2	327.8	333.9	314.5 (18.2)
		NCP	$gC.m^{-2}.yr^{-1}$	22.1	38.6	27.5	36.2	23.2	37.4	34.3	31.2 (6.9)
		NPP	$gC.m^{-2}.yr^{-1}$	90.5	109.6	106.7	123.9	114.9	129.6	132.5	115.0 (14.7)
		POC vertical export at 150 m	$gC.m^{-2}.yr^{-1}$	-7.8	-14.2	-9.7	-16.4	-8.1	-14.3	-12.8	-11.9 (3.4)
		DOC vertical export at 150 m	$gC.m^{-2}.yr^{-1}$	-1.1	-6.8	-3.6	-8.8	-2.2	-6.5	-5.5	-4.9 (2.8)
		OC vertical export at 150 m	$gC.m^{-2}.yr^{-1}$	-8.9	-21	-13.3	-25.2	-10.3	-20.8	-18.3	-16.8 (6.2)
		OC lateral export	$gC.m^{-2}.yr^{-1}$	-13.1	-16.3	-13.5	-10.6	-13.6	-14.7	-16.8	-14.1 (2.1)
		OC inventory variation	$gC.m^{-2}.yr^{-1}$	0.1	1.4	0.7	0.4	-0.6	2	-0.8	0.44 (1)
Intermediate layer (150 -	**Annual**	CR	$gC.m^{-2}.yr^{-1}$	-4.6	-11.5	-5.9	-11.5	-5.2	-10.7	-9.8	-8.5 (3.1)

https://doi.org/10.5194/bg-2022-216
Preprint. Discussion started: 21 November 2022

400 m)		POC vertical export at 400 m	$gC.m^{-2}.yr^{-1}$	1.5	1.9	1.7	2.3	1.7	2.2	2.1	1.9 (0.3)
		DOC vertical export at 400 m	$gC.m^{-2}.yr^{-1}$	-1.3	-1.1	-0.9	-0.7	-0.8	-0.6	-1.0	-0.9 (0.2)
		OC vertical export at 400 m	$gC.m^{-2}.yr^{-1}$	0.2	0.8	0.8	1.6	0.9	1.6	1.1	1.0 (0.5)
		OC lateral export	$gC.m^{-2}.yr^{-1}$	-4.0	-9.1	-6.3	-12.3	-4.6	-8.2	-7.7	-7.5 (2.8)
		OC inventory variation	$gC.m^{-2}.yr^{-1}$	0.02	-0.4	0.3	-0.2	-0.3	0.3	-0.4	-0.1 (0.3)

45